

Exact Prescribed-Time Prescribed-Accuracy Control for Spacecraft under Dual Reaction Wheel Saturation

First A. Author * and Second B. Author Jr.[†]
Business or Academic Affiliation 1, City, State, Zip Code

Third C. Author[‡]
Business or Academic Affiliation 2, City, Province, Zip Code, Country

Fourth D. Author[§]
Business or Academic Affiliation 2, City, State, Zip Code

This paper proposes an Exact Prescribed-Time Prescribed-Accuracy Control (EPTPAC) framework for rigid spacecraft equipped with reaction wheels subject to dual saturation, which includes the torque saturation and the wheel angular-momentum saturation. The proposed scheme guarantees that attitude tracking errors converge to a user-specified accuracy neighborhood exactly at a user-defined terminal time T_f , while strictly respecting the dual saturation constraints throughout the maneuver. The approach employs a two-loop architecture: an outer-loop trajectory planner generates a dynamically feasible reference that satisfies the dual saturation bounds and reaches the target state exactly at T_f ; an inner-loop nonsingular prescribed-time tracking controller then drives the tracking errors into the prescribed accuracy neighborhood before T_f with bounded control gain. A systematic parameter-synthesis procedure is also developed to coordinate the two loops and ensure closed-loop feasibility under bounded disturbances. Numerical simulations of large-angle maneuvers demonstrate exact terminal-time convergence, robustness, and strict compliance with dual saturation constraints.

Nomenclature

Roman Symbols

d	lumped disturbance torque [N · m]
d_{\max}	bound on $\ d(t)\ $ [N · m]
h_w	reaction-wheel angular momentum (body frame) [kg · m ² /s]
$h_{w,i,\max}$	maximum allowable wheel momentum (axis i) [kg · m ² /s]

*Insert Job Title, Department Name, Address/Mail Stop, and AIAA Member Grade (if any) for first author.

[†]Insert Job Title, Department Name, Address/Mail Stop, and AIAA Member Grade (if any) for second author.

[‡]Insert Job Title, Department Name, Address/Mail Stop, and AIAA Member Grade (if any) for third author.

[§]Insert Job Title, Department Name, Address/Mail Stop, and AIAA Member Grade (if any) for fourth author (etc.).

$\mathbf{h}_{w,0}$	initial wheel momentum [$\text{kg} \cdot \text{m}^2/\text{s}$]
\mathbf{H}	total angular momentum, $\mathbf{H} = \mathbf{J}\boldsymbol{\omega} + \mathbf{h}_w$ [$\text{kg} \cdot \text{m}^2/\text{s}$]
H_{\max}	bound on $\ \mathbf{H}(t)\ $ over $[0, T_f]$ [$\text{kg} \cdot \text{m}^2/\text{s}$]
\mathbf{J}	spacecraft inertia matrix [$\text{kg} \cdot \text{m}^2$]
$\lambda_{\min}(\mathbf{J}), \lambda_{\max}(\mathbf{J})$	minimum/maximum eigenvalues of \mathbf{J} [$\text{kg} \cdot \text{m}^2$]
$\mathbf{R}(\boldsymbol{\sigma}_e)$	direction cosine matrix associated with $\boldsymbol{\sigma}_e$ [-]
$\mathbf{G}(\boldsymbol{\sigma})$	MRP kinematic matrix [-]
T_f	user-specified terminal time [s]
T_{p1}, T_{p2}	prescribed convergence times (attitude/sliding variable) [s]
τ	control torque applied to spacecraft body [$\text{N} \cdot \text{m}$]
$\tau_{i,\max}$	maximum allowable torque (axis i) [$\text{N} \cdot \text{m}$]
τ_{ref}	planned reference torque from the outer-loop OCP [$\text{N} \cdot \text{m}$]
$\boldsymbol{\omega}$	spacecraft angular velocity (body frame) [rad/s]
$\boldsymbol{\omega}_d$	reference angular velocity [rad/s]
$\boldsymbol{\omega}_e$	angular-velocity tracking error [rad/s]
$\omega_{d,\max}$	bound on $\ \boldsymbol{\omega}_d(t)\ $ on $[0, T_f]$ [rad/s]
$\dot{\omega}_{d,\max}$	bound on $\ \dot{\boldsymbol{\omega}}_d(t)\ $ on $[0, T_f]$ [rad/s ²]
$\boldsymbol{\sigma}$	Modified Rodrigues Parameters (MRPs) [-]
$\boldsymbol{\sigma}_d$	reference MRPs [-]
$\boldsymbol{\sigma}_e$	attitude tracking error in MRPs [-]
μ_i	row-sum coefficient of inertia, $\mu_i = \sum_{j=1}^3 J_{ij} $ [$\text{kg} \cdot \text{m}^2$]
λ	OCP smoothness weight in (22) [-]

Greek Symbols

η	exponent in prescribed-time law, $0 < \eta < 1$ [-]
$\varepsilon_1, \varepsilon_2$	prescribed accuracy tolerances (attitude/sliding variable) [-]
$\varepsilon_{\text{mission}}$	mission-level attitude accuracy requirement [-]
α_1, α_2	tunable gains in prescribed-time laws [-]
γ_u, γ_h	constraint-tightening margins (torque/momenta) [-]

I. Introduction

Time-critical spacecraft missions, such as rendezvous, docking, and formation reconfiguration, require the attitude to reach a commanded state at an exact user-specified terminal time T_f , which is dictated by orbital geometry,

communication windows, or multi-vehicle coordination requirements [1–3]. This terminal-time requirement becomes substantially more challenging for reaction-wheel spacecraft that operate under dual reaction-wheel saturation, which includes the torque saturation and the wheel angular-momentum saturation. Hereafter, dual saturation denotes the joint torque and momentum saturation of reaction wheels. During large-angle maneuvers, wheel momentum can saturate even when torque commands stay within bounds, which makes many analytically valid controllers physically unrealizable. Accordingly, a practical terminal-time control strategy should guarantee arrival at $t = T_f$ while strictly respecting dual saturation throughout the maneuver.

To overcome the sluggishness of asymptotic designs, finite-time control (FTC) [4, 5] and fixed-time control (FxTC) [6, 7] have been widely studied. FTC guarantees convergence in finite time, but the settling time depends on initial conditions, which weakens timing predictability. FxTC removes this dependence, but it typically provides a conservative upper bound that cannot be aligned with a mission-specified terminal time. These limitations motivate prescribed-time control, where the convergence time enters explicitly as a design parameter.

Existing prescribed-time methods can be broadly categorized into three lines. The first embeds the prescribed time into Lyapunov inequalities using exponential and power terms [8, 9] and has been applied to robotic tracking, launch-vehicle attitude control, flexible spacecraft, and formation flying [3, 10–15]. These designs are markedly conservative, often driving convergence well before the specified time and inducing very large initial torque demands. The second line employs time-varying high-gain feedback with time-warping transformations [5, 16] and has been used in consensus and robust tracking [17–20]. Compared with the first line, conservatism is reduced, but the gain typically grows rapidly as time approaches T_f , which makes the controller vulnerable to saturation and noise. In practice, truncation or smoothing is introduced to keep gains bounded [18, 21], but this comes at the cost of performance, since terminal-time tightness and tracking accuracy are generally weakened. The third line leverages periodic delayed feedback to obtain smooth prescribed-time stabilization [22–24]. Although it avoids singularities, it can be sensitive to disturbances and may induce inefficient attitude reversals, which increases momentum usage. Despite these advances, existing PTC approaches for reaction-wheel spacecraft still exhibit two fundamental shortcomings that hinder their use in time-critical missions.

First, a number of PTC designs are conservative [3, 16, 18]. They guarantee convergence no later than prescribed time T_f , yet the closed-loop response often settles significantly earlier, as reported in [3] where the prescribed time is set to 500 s but the convergence occurs at about 250 s. Such premature convergence is unacceptable in missions with hard terminal-time constraints. For example, in on-orbit assembly or formation reconfiguration scenarios, arriving much ahead of schedule can result in task conflicts or physical interference with other vehicles that are scheduled to operate in the same workspace. Early settling also induces unnecessarily large torque transients and wastes momentum resources, which is particularly undesirable for reaction-wheel spacecraft.

Second, physical realizability under dual saturation remains insufficiently addressed. Although torque saturation has

been incorporated into certain PTC designs [2, 15, 20], the joint treatment of dual saturation is rarely considered. More critically, the prescribed terminal time T_f is often selected as a free tuning parameter, ignoring that it is fundamentally lower-bounded by the actuator’s torque and momentum capacities together with the maneuver’s kinematic demands. For large-angle attitude reconfigurations, this minimum feasible time can be substantial; prescribing a shorter horizon may render the control law infeasible or cause hidden constraint violations, even if the nominal design appears mathematically valid.

Optimization-based trajectory planning can provide a potential solution because it can explicitly embed torque and momentum limits and enforce terminal-time boundary conditions by construction [25–28]. However, these approaches are applied in an open-loop manner. Under disturbances or modeling errors, tracking can drift away from the planned trajectory and terminal-time accuracy is not guaranteed. Some studies have combined optimization with feedback control to improve practical performance [29, 30], but aggressive maneuvers and significant disturbances can still lead to noticeable deviation, and terminal-time tracking guarantees remain largely unavailable.

Motivated by these observations, this paper proposes a EPTPAC framework built on a two-loop architecture. The outer loop generates a physically realizable reference trajectory that respects dual saturation and reaches the target state exactly at the user-specified terminal time T_f . The inner loop designs a nonsingular prescribed-time sliding-mode tracking controller, which guarantees that the spacecraft tracks the planned trajectory and drives the attitude and angular-velocity errors into a user-prescribed accuracy neighborhood before T_f , without gain blow-up. Together, the two loops ensure terminal-time attitude maneuvers that satisfy dual saturation while achieving user-specified accuracy at the mission time. In addition, a systematic parameter-synthesis procedure is provided to coordinate the two loops and maintain feasibility in the presence of disturbances.

The main contributions of this paper are summarized as follows:

- 1) The framework guarantees that attitude tracking errors enter a user-specified accuracy neighborhood exactly at the prescribed terminal time T_f , eliminating premature convergence.
- 2) The framework guarantees physical realizability under dual saturation, ensuring the prescribed terminal time T_f is actually achievable.
- 3) The framework establishes a new prescribed-time control paradigm based on an extensible two-loop architecture that jointly ensures trajectory feasibility and prescribed-time tracking performance.

The remainder of this paper is organized as follows. Section II formulates the spacecraft attitude dynamics with reaction wheels and the dual saturation constraints, and it reviews practical prescribed-time stability tools. Section III presents the proposed framework, including trajectory planning, controller design, and synthesis rules. Section IV reports simulation studies for large-angle maneuvers under significant disturbances. Section V concludes the paper and discusses future work.

II. Problem Description and Preliminaries

A. Problem Description

Let \mathbb{R} denote the set of real numbers. For vectors and matrices, $(\cdot)^T$ denotes transpose, $\|\cdot\|$ denotes the Euclidean norm, and \mathbf{I}_n denotes the $n \times n$ identity matrix. For a symmetric positive definite matrix \mathbf{A} , $\lambda_{\min}(\mathbf{A})$ and $\lambda_{\max}(\mathbf{A})$ denote its minimum and maximum eigenvalues, respectively. For any $\mathbf{a} = [a_1, a_2, a_3]^T \in \mathbb{R}^3$, define

$$\mathbf{a}^\times \triangleq \begin{bmatrix} 0 & -a_3 & a_2 \\ a_3 & 0 & -a_1 \\ -a_2 & a_1 & 0 \end{bmatrix}$$

The attitude kinematics and dynamics of a rigid spacecraft with reaction wheels can be written as

$$\dot{\boldsymbol{\sigma}} = \mathbf{G}(\boldsymbol{\sigma})\boldsymbol{\omega}, \quad \mathbf{G}(\boldsymbol{\sigma}) = \frac{1}{4} [(1 - \|\boldsymbol{\sigma}\|^2)\mathbf{I}_3 + 2\boldsymbol{\sigma}^\times + 2\boldsymbol{\sigma}\boldsymbol{\sigma}^T] \quad (1)$$

$$\mathbf{J}\dot{\boldsymbol{\omega}} + \boldsymbol{\omega}^\times(\mathbf{J}\boldsymbol{\omega} + \mathbf{h}_w) = \mathbf{d} + \boldsymbol{\tau}, \quad \boldsymbol{\tau} = -\dot{\mathbf{h}}_w \quad (2)$$

where $\boldsymbol{\sigma} \in \mathbb{R}^3$ denotes the modified Rodrigues parameters (MRPs) of the spacecraft attitude, $\boldsymbol{\omega} \in \mathbb{R}^3$ is the body angular velocity with respect to the inertial frame expressed in the body frame, $\mathbf{J} \in \mathbb{R}^{3 \times 3}$ is the constant symmetric positive definite inertia matrix, $\mathbf{h}_w \in \mathbb{R}^3$ is the reaction-wheel angular momentum expressed in the body frame, $\boldsymbol{\tau} \in \mathbb{R}^3$ is the control torque applied to the spacecraft body, and $\mathbf{d} \in \mathbb{R}^3$ denotes the lumped disturbance torque.

For clarity of exposition, a three-axis reaction-wheel cluster is considered, where the wheel axes are aligned with the body principal axes. The reaction-wheel actuators are subject to dual saturation. For each axis $i \in \{1, 2, 3\}$, the following constraints hold:

$$|\tau_i(t)| \leq \tau_{i,\max} \quad (3)$$

$$|h_{w,i}(t)| \leq h_{w,i,\max} \quad (4)$$

where τ_i and $h_{w,i}$ denote the i th components of the control torque $\boldsymbol{\tau}$ and wheel angular momentum \mathbf{h}_w , respectively, and $\tau_{i,\max} > 0$ and $h_{w,i,\max} > 0$ are the corresponding component-wise bounds.

Let $\boldsymbol{\sigma}_d \in \mathbb{R}^3$ and $\boldsymbol{\omega}_d \in \mathbb{R}^3$ denote the desired attitude MRP and angular velocity, respectively. The attitude tracking error $\boldsymbol{\sigma}_e \in \mathbb{R}^3$ is defined as the MRP representation of the relative rotation from the desired frame to the current body frame:

$$\boldsymbol{\sigma}_e = \frac{(1 - \|\boldsymbol{\sigma}_d\|^2)\boldsymbol{\sigma} - (1 - \|\boldsymbol{\sigma}\|^2)\boldsymbol{\sigma}_d + 2\boldsymbol{\sigma}_d^\times\boldsymbol{\sigma}}{1 + \|\boldsymbol{\sigma}\|^2\|\boldsymbol{\sigma}_d\|^2 + 2\boldsymbol{\sigma}^T\boldsymbol{\sigma}_d} \quad (5)$$

$$\omega_e = \omega - \mathbf{R}(\sigma_e)\omega_d \quad (6)$$

where $\mathbf{R}(\sigma_e) \in \mathbb{R}^{3 \times 3}$ is the direction cosine matrix associated with σ_e , given by

$$\mathbf{R}(\sigma_e) = \mathbf{I}_3 + \frac{8\sigma_e^\times \sigma_e^\times - 4(1 - \sigma_e^T \sigma_e)\sigma_e^\times}{(1 + \sigma_e^T \sigma_e)^2} \quad (7)$$

To avoid the MRP singularity at 360° , the standard shadow-set switching can be applied; hence, the error representation can be kept in the practical region $\|\sigma_e(t)\| < 1$.

Based on the above definitions, the tracking error kinematics and dynamics can be written as

$$\dot{\sigma}_e = \mathbf{G}(\sigma_e)\omega_e, \quad \mathbf{G}(\sigma_e) = \frac{1}{4} [(1 - \|\sigma_e\|^2)\mathbf{I}_3 + 2\sigma_e^\times + 2\sigma_e\sigma_e^T] \quad (8)$$

$$\mathbf{J}\dot{\omega}_e = \boldsymbol{\tau} + \mathbf{d} + \mathbf{f} \quad (9)$$

where the 2-norm of the kinematic matrix $\mathbf{G}(\sigma_e)$ satisfies $\|\mathbf{G}(\sigma_e)\| = \frac{1+\|\sigma_e\|^2}{4}$. Consequently, for all $\|\sigma_e\| < 1$, it follows that

$$\frac{1}{4} \leq \|\mathbf{G}(\sigma_e)\| < \frac{1}{2}. \quad (10)$$

Here, $\mathbf{f} \in \mathbb{R}^3$ is a known feedforward term determined by the measured states and the reference signals, given by

$$\mathbf{f} := -\omega^\times(\mathbf{J}\omega + \mathbf{h}_w) + \mathbf{J}\omega_e^\times \mathbf{R}(\sigma_e)\omega_d + \mathbf{J}\mathbf{R}(\sigma_e)\dot{\omega}_d.$$

The following assumptions are imposed.

Assumption 1. *The user-specified terminal time $T_f > 0$ satisfies*

$$T_f \geq T_{f,\min} \quad (11)$$

where $T_{f,\min} > 0$ is the minimum maneuver time required to transfer the spacecraft from the initial state to the target state under the component-wise constraints (3)–(4). Consequently, there exists a dynamically feasible reference trajectory (σ_d, ω_d) on $[0, T_f]$ with bounded angular velocity and angular acceleration: there exist known constants $\omega_{d,\max} > 0$ and $\dot{\omega}_{d,\max} > 0$ such that

$$\|\omega_d(t)\| \leq \omega_{d,\max}, \quad \|\dot{\omega}_d(t)\| \leq \dot{\omega}_{d,\max}, \quad \forall t \in [0, T_f] \quad (12)$$

Assumption 2. The lumped disturbance torque \mathbf{d} is bounded. Namely, there exists a known constant $d_{\max} > 0$ such that

$$\|\mathbf{d}(t)\| \leq d_{\max}, \quad \forall t \in [0, T_f] \quad (13)$$

Assumption 3. Let $\mathbf{H}(t) := \mathbf{J}\boldsymbol{\omega}(t) + \mathbf{h}_w(t)$ denote the total angular momentum in the body frame. The total angular momentum satisfies

$$\|\mathbf{H}(t)\| \leq H_0 + H_{\max}, \quad \forall t \in [0, T_f], \quad (14)$$

where $H_0 = \|\mathbf{H}(0)\| \geq 0$ is the known initial total angular momentum, and $H_{\max} > 0$ is a known bound on the momentum drift induced by external disturbances over $[0, T_f]$.

The control objective is to design a EPTPAC scheme for a given terminal time $T_f > 0$ and a mission-required accuracy $\varepsilon_{\text{mission}} > 0$ such that: (i) the dual saturation constraints (3)–(4) hold for all $t \in [0, T_f]$; (ii) the spacecraft reaches the desired terminal state at $t = T_f$ by tracking the planned reference; and (iii) the tracking errors $(\sigma_e, \boldsymbol{\omega}_e)$ enter a neighborhood of the origin with radius no larger than $\varepsilon_{\text{mission}}$ before T_f and remain bounded thereafter. The overall framework is shown in Fig. 1.

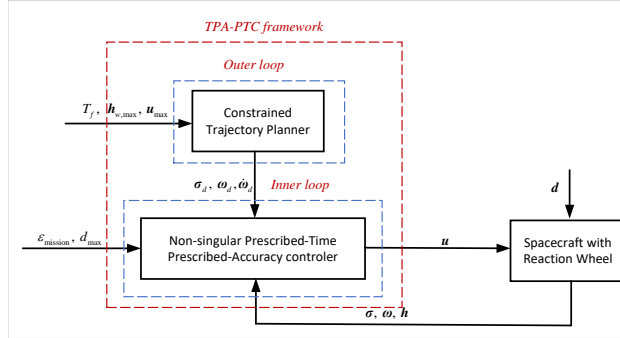


Fig. 1 The EPTPAC framework

B. Preliminaries

This subsection summarizes basic tools on prescribed-time stability that will be used in the subsequent analysis and controller design. These results are standard and are included only for completeness.

Consider the nonlinear system

$$\dot{\mathbf{x}} = \mathbf{g}(\mathbf{x}, t) \quad (15)$$

where $\mathbf{x} \in \mathbb{R}^n$ and $\mathbf{g}(\mathbf{x}, t)$ is locally Lipschitz in \mathbf{x} , with $\mathbf{g}(\mathbf{0}, t) = \mathbf{0}$. Given a constant $T_p > 0$, the origin is said to be prescribed-time stable if, for any initial condition $\mathbf{x}(0) = \mathbf{x}_0$, the solution exists and reaches the origin in finite time $T(\mathbf{x}_0) \leq T_p$.

Lemma 1 ([10]). Suppose there exists a Lyapunov function $V(\mathbf{x})$ of system (15) such that

$$\dot{V} \leq -\frac{\pi}{\eta T_p} \left(V^{1-\frac{\eta}{2}} + V^{1+\frac{\eta}{2}} \right) \quad (16)$$

where $0 < \eta < 1$ and $T_p > 0$ are given constants. Then the state converges to the origin within time T_p , i.e., the origin is prescribed-time stable.

Theorem 1. Suppose there exists a Lyapunov function $V(\mathbf{x})$ for system (15) such that

$$\dot{V} \leq \delta V^{\frac{1}{2}} - \frac{\pi}{\eta T_p} \left[(1 + \alpha) V^{1-\frac{\eta}{2}} + V^{1+\frac{\eta}{2}} \right] \quad (17)$$

where $\delta > 0$, $\alpha > 0$, $0 < \eta < 1$, and $T_p > 0$ are constants. Then, for any initial condition, the trajectory enters the set

$$V \leq V_{\delta}^*, \quad V_{\delta}^* := \left(\frac{\delta \eta T_p}{\pi \alpha} \right)^{\frac{2}{1-\eta}} \quad (18)$$

in no more than T_p seconds and remains in it thereafter.

Proof: Let $K := \frac{\pi}{\eta T_p} > 0$ and let V_{δ}^* be defined in (18). From (17),

$$\dot{V} \leq \delta V^{\frac{1}{2}} - K \left[(1 + \alpha) V^{1-\frac{\eta}{2}} + V^{1+\frac{\eta}{2}} \right] \quad (19)$$

By construction, $V = V_{\delta}^*$ satisfies $\delta V^{1/2} = K \alpha V^{1-\eta/2}$. Moreover, for all $V \geq V_{\delta}^*$, the function $V^{-(1-\eta)/2}$ is decreasing, hence $\delta V^{1/2} \leq K \alpha V^{1-\eta/2}$, and therefore

$$\dot{V} \leq -K \left(V^{1-\frac{\eta}{2}} + V^{1+\frac{\eta}{2}} \right), \quad \forall V \geq V_{\delta}^*. \quad (20)$$

By Lemma 1, any trajectory with $V(0) > V_{\delta}^*$ reaches the set $\{V \leq V_{\delta}^*\}$ within at most T_p . Finally, note that at the boundary $V = V_{\delta}^*$ we have $\dot{V} \leq -K \left(V^{1-\frac{\eta}{2}} + V^{1+\frac{\eta}{2}} \right) < 0$, which implies that the set $\{V \leq V_{\delta}^*\}$ is forward invariant. This completes the proof. \square

Lemma 2. For any vector $\mathbf{x} \in \mathbb{R}^n$ satisfying $\|\mathbf{x}\| \geq \varepsilon$ with $\varepsilon > 0$, and any $0 < \eta < 1$, the following inequalities hold:

$$\frac{\|\mathbf{x}\|^2}{(\|\mathbf{x}\| + \varepsilon)^\eta} \geq \frac{1}{2^\eta} \|\mathbf{x}\|^{2-\eta}, \quad \frac{\|\mathbf{x}\|^2}{(\|\mathbf{x}\| + \varepsilon)^{-\eta}} \geq \|\mathbf{x}\|^{2+\eta} \quad (21)$$

III. Main Results

A. Outer-Loop Trajectory Planning Under Dual Saturation

To enforce exact arrival at the user-specified terminal time $T_f > 0$, an offline reference trajectory $(\sigma_d(t), \omega_d(t))$ is constructed by solving a constrained optimal control problem (OCP) over $[0, T_f]$. The OCP explicitly embeds the spacecraft kinematics and dynamics (1)–(2) together with the dual saturation constraints (3)–(4), thereby ensuring that the reference is dynamically consistent and actuator-feasible.

Specifically, the OCP is formulated as

$$\begin{aligned} \min_{\tau_{\text{ref}}(\cdot), \Delta\sigma_0} \quad J &= \int_0^{T_f} \left(\|\tau_{\text{ref}}(t)\|^2 + \lambda \|\dot{\tau}_{\text{ref}}(t)\|^2 \right) dt \\ \text{s.t.} \quad \dot{\sigma}(t) &= \mathbf{G}(\sigma(t))\omega(t), \\ \mathbf{J}\dot{\omega}(t) + \omega(t)^{\times}(\mathbf{J}\omega(t) + \mathbf{h}_w(t)) &= \tau_{\text{ref}}(t), \\ \dot{\mathbf{h}}_w(t) &= -\tau_{\text{ref}}(t), \quad \mathbf{h}_w(0) = \mathbf{h}_{w,0}, \\ \sigma(0) &= \sigma_0, \\ \omega(0) &= \omega_0, \\ \sigma(T_f) &= \sigma_{\text{target}}, \quad \omega(T_f) = \omega_{\text{target}}, \\ |\tau_{\text{ref},i}(t)| &\leq (1 - \gamma_u) \tau_{i,\text{max}}, \quad i \in \{1, 2, 3\}, \\ |h_{w,i}(t)| &\leq (1 - \gamma_h) h_{w,i,\text{max}}, \quad i \in \{1, 2, 3\}. \end{aligned} \tag{22}$$

Here $\lambda > 0$ weights control effort and smoothness, while $\gamma_u, \gamma_h \in (0, 1)$ tighten the actuator bounds to reserve headroom for inner-loop tracking and disturbance rejection.

The OCP is solved offline using the Gauss pseudospectral method GPOPS-II [31], producing nodal torques $\{\tau_i\}_{i=0}^N$ at nodes $\{t_i\}_{i=0}^N$. A continuous-time torque command is obtained via piecewise-linear interpolation:

$$\tilde{\tau}(t) = \tau_i + \frac{t - t_i}{t_{i+1} - t_i} (\tau_{i+1} - \tau_i), \quad t \in [t_i, t_{i+1}], \quad i = 0, \dots, N-1. \tag{23}$$

The interpolated torque $\tilde{\tau}(t)$ is then integrated through (1)–(2) to reconstruct a dynamically consistent reference trajectory $(\sigma_d(t), \omega_d(t))$. Since each component satisfies $|\tau_i(t_i)| \leq (1 - \gamma_u) \tau_{i,\text{max}}$ and $|\tau_i(t_{i+1})| \leq (1 - \gamma_u) \tau_{i,\text{max}}$, the piecewise-linear interpolation implies $|\tilde{\tau}_i(t)| \leq (1 - \gamma_u) \tau_{i,\text{max}}$ for all $t \in [t_i, t_{i+1}]$.

Remark 1. *The outer-loop planner is not posed as a standalone contribution in optimal control. Its role is to embed the dual saturation limits and terminal boundary conditions into reference generation, providing a physically realizable, time-anchored trajectory for the inner-loop prescribed-time tracker.*

Remark 2. Assumption 1 implies the existence of a minimum feasible maneuver time $T_{f,\min}$ under the dual saturation constraints. A conservative estimate can be obtained via a bang-bang (time-optimal) construction under component-wise torque limits; an explicit procedure is provided in Appendix A.

B. Inner-Loop Nonsingular Prescribed-Time Tracking Control

To facilitate a nonsingular prescribed-accuracy prescribed-time design, this section introduces the following sliding surface that couples the attitude and angular-velocity tracking errors.

Define the sliding surface as

$$s = \omega_e + Q(\sigma_e), \quad (24)$$

where

$$Q(\sigma_e) = c_1 k_1 \frac{\sigma_e}{(\|\sigma_e\| + \varepsilon_1)^\eta} + c_1 k_2 \frac{\sigma_e}{(\|\sigma_e\| + \varepsilon_1)^{-\eta}}, \quad (25)$$

with constants $0 < \eta < 1$, $\varepsilon_1 > 0$,

$$c_1 = \frac{\pi}{\eta T_{p1}}, \quad k_1 = (1 + \alpha_1) 2^{1+\frac{3}{2}\eta}, \quad k_2 = 2^{1-\frac{\eta}{2}},$$

where $T_{p1} > 0$ and $\alpha_1 > 0$.

Theorem 2. If the sliding surface $s(t)$ converges to the bounded set $\|s(t)\| \leq s_{\max}$. Then the attitude error $\sigma_e(t)$ will converge within time T_{p1} to the set

$$\|\sigma_e(t)\| \leq \max \{\varepsilon_{\delta_1}, \varepsilon_1\} \quad (26)$$

where

$$\varepsilon_{\delta_1} := \sqrt{2} \left(\frac{\delta_1 \eta T_{p1}}{\pi \alpha_1} \right)^{\frac{1}{1-\eta}}, \quad \delta_1 := \frac{\sqrt{2}}{2} s_{\max}. \quad (27)$$

Proof. Consider the Lyapunov function candidate

$$V_1 = \frac{1}{2} \|\sigma_e\|^2. \quad (28)$$

For t such that $\|s(t)\| \leq s_{\max}$, differentiating along the error kinematics $\dot{\sigma}_e = G(\sigma_e)\omega_e$ and substituting $\omega_e = s - Q(\sigma_e)$ yields

$$\begin{aligned} \dot{V}_1 &= \sigma_e^\top G(\sigma_e)(s - Q(\sigma_e)) \\ &\leq \|G(\sigma_e)\| \|\sigma_e\| s_{\max} - \sigma_e^\top G(\sigma_e) Q(\sigma_e). \end{aligned} \quad (29)$$

From (10), $\|\mathbf{G}(\boldsymbol{\sigma}_e)\| < \frac{1}{2}$ for $\|\boldsymbol{\sigma}_e\| < 1$. Assuming $\|\boldsymbol{\sigma}_e\| \geq \varepsilon_1$, Lemma 2 gives

$$\frac{\|\boldsymbol{\sigma}_e\|^2}{(\|\boldsymbol{\sigma}_e\| + \varepsilon_1)^\eta} \geq \frac{1}{2^\eta} \|\boldsymbol{\sigma}_e\|^{2-\eta}, \quad \frac{\|\boldsymbol{\sigma}_e\|^2}{(\|\boldsymbol{\sigma}_e\| + \varepsilon_1)^{-\eta}} \geq \|\boldsymbol{\sigma}_e\|^{2+\eta}.$$

Thus,

$$\begin{aligned} \dot{V}_1 &\leq \frac{1}{2} \|\boldsymbol{\sigma}_e\| s_{\max} - \frac{c_1}{4} \left[k_1 \frac{\|\boldsymbol{\sigma}_e\|^2}{(\|\boldsymbol{\sigma}_e\| + \varepsilon_1)^\eta} + k_2 \frac{\|\boldsymbol{\sigma}_e\|^2}{(\|\boldsymbol{\sigma}_e\| + \varepsilon_1)^{-\eta}} \right] \\ &\leq \frac{\sqrt{2}}{2} V_1^{1/2} s_{\max} - \frac{c_1}{4} \left[k_1 2^{-\eta} (2V_1)^{1-\eta/2} + k_2 (2V_1)^{1+\eta/2} \right]. \end{aligned} \quad (30)$$

Substituting $c_1 = \frac{\pi}{\eta T_{p1}}$, $k_1 = (1 + \alpha_1) 2^{1+\frac{3}{2}\eta}$, and $k_2 = 2^{1-\frac{\eta}{2}}$ yields

$$\dot{V}_1 \leq \delta_1 V_1^{1/2} - \frac{\pi}{\eta T_{p1}} \left[(1 + \alpha_1) V_1^{1-\eta/2} + V_1^{1+\eta/2} \right]. \quad (31)$$

This satisfies the condition of Theorem 1. Hence, $V_1(t)$ converges within time T_{p1} to

$$V_1 \leq \frac{1}{2} \varepsilon_{\delta_1}^2. \quad (32)$$

Since $V_1 = \frac{1}{2} \|\boldsymbol{\sigma}_e\|^2$, it follows that $\|\boldsymbol{\sigma}_e(t)\| \leq \varepsilon_{\delta_1}$. Moreover, the regularization ensures that the set $\{\|\boldsymbol{\sigma}_e\| \leq \varepsilon_1\}$ is positively invariant. Combining both cases yields the stated bound $\|\boldsymbol{\sigma}_e(t)\| \leq \max\{\varepsilon_{\delta_1}, \varepsilon_1\}$. \square

Remark 3. The parameter ε_{δ_1} depends inversely on $\alpha_1^{1/(1-\eta)}$. Therefore, for any fixed s_{\max} and T_{p1} , one can always choose a appropriate $\alpha_1 > 0$ such that $\varepsilon_{\delta_1} < \varepsilon_1$. In this case, the ultimate convergence bound becomes $\|\boldsymbol{\sigma}_e(t)\| \leq \varepsilon_1$, and the user-specified tolerance ε_1 fully determines the practical accuracy of the maneuver.

Remark 4. The parameter $\varepsilon_1 > 0$ serves two purposes: (i) it eliminates the singularity in $\mathbf{Q}(\boldsymbol{\sigma}_e)$ as $\|\boldsymbol{\sigma}_e\| \rightarrow 0$, ensuring a smooth and bounded control law; and (ii) it provides a direct, user-adjustable interface for specifying the desired convergence tolerance. In practical applications, exact zero error is neither achievable nor necessary; ε_1 allows engineers to encode mission-level precision requirements directly into the controller design.

Based on the above surface, construct a prescribed-time inner-loop torque command consisting of a computable feedforward cancellation term and a dominant prescribed-time stabilizing term. The resulting inner-loop control law is given by

$$\boldsymbol{\tau} = -\mathbf{f}(t) - \mathbf{J}\dot{\mathbf{Q}}(\boldsymbol{\sigma}_e) + \boldsymbol{\tau}_c, \quad (33)$$

where $f(t)$ is the known nonlinear term defined in (9), and the prescribed-time dominant term τ_c is given by

$$\tau_c = -c_2 \left[k_3 \frac{s}{(\|s\| + \varepsilon_2)^\eta} + k_4 \frac{s}{(\|s\| + \varepsilon_2)^{-\eta}} \right], \quad (34)$$

with design parameters $0 < \eta < 1$, $\varepsilon_2 > 0$, and

$$c_2 = \frac{\pi}{\eta T_{p2}}, \quad k_3 = (1 + \alpha_2) 2^{-1+\frac{3}{2}\eta} \lambda_{\max}(\mathbf{J})^{1-\frac{\eta}{2}}, \quad k_4 = 2^{-1-\frac{\eta}{2}} \lambda_{\max}(\mathbf{J})^{1+\frac{\eta}{2}}.$$

Here, $T_{p2} > 0$ is the prescribed convergence time for the sliding surface, and $\alpha_2 > 0$ is a tunable gain.

Substituting the control law into the attitude error dynamics (9) and using the definition of s , the closed-loop sliding surface dynamics are obtained. Left-multiplying by \mathbf{J} yields

$$\mathbf{J}\dot{s} = \tau_c + \mathbf{d}(t) \quad (35)$$

Theorem 3. *Under Assumption 2, the sliding variable $s(t)$ converges to the bounded set*

$$\|s(t)\| \leq \max \{ \varepsilon_{\delta_2}, \varepsilon_2 \}, \quad (36)$$

where

$$\varepsilon_{\delta_2} := \sqrt{2} \left(\frac{\delta_2 \eta T_{p2}}{\pi \alpha_2} \right)^{\frac{1}{1-\eta}}, \quad \delta_2 := d_{\max} \sqrt{\frac{2}{\lambda_{\min}(\mathbf{J})}}. \quad (37)$$

Proof. Consider the Lyapunov function

$$V_2 = \frac{1}{2} s^\top \mathbf{J} s. \quad (38)$$

Its time derivative along the closed-loop dynamics (35) is

$$\dot{V}_2 = s^\top \tau_c + s^\top \mathbf{d}(t). \quad (39)$$

For the disturbance term, using $\|s\| \leq \sqrt{2V_2/\lambda_{\min}(\mathbf{J})}$ yields

$$s^\top \mathbf{d}(t) \leq \|s\| d_{\max} \leq \delta_2 V_2^{1/2}, \quad \delta_2 := d_{\max} \sqrt{\frac{2}{\lambda_{\min}(\mathbf{J})}} \quad (40)$$

For the control term, assuming $\|s\| \geq \varepsilon_2$, Lemma 2 gives

$$\frac{\|s\|^2}{(\|s\| + \varepsilon_2)^\eta} \geq \frac{1}{2^\eta} \|s\|^{2-\eta}, \quad \frac{\|s\|^2}{(\|s\| + \varepsilon_2)^{-\eta}} \geq \|s\|^{2+\eta}.$$

Thus,

$$\begin{aligned}
\mathbf{s}^\top \boldsymbol{\tau}_c &= -c_2 \left[k_3 \frac{\|\mathbf{s}\|^2}{(\|\mathbf{s}\| + \varepsilon_2)^\eta} + k_4 \frac{\|\mathbf{s}\|^2}{(\|\mathbf{s}\| + \varepsilon_2)^{-\eta}} \right] \\
&\leq -c_2 \left[k_3 2^{-\eta} \|\mathbf{s}\|^{2-\eta} + k_4 \|\mathbf{s}\|^{2+\eta} \right] \\
&\leq -\frac{\pi}{\eta T_{p2}} \left[(1 + \alpha_2) V_2^{1-\eta/2} + V_2^{1+\eta/2} \right], \tag{41}
\end{aligned}$$

where in the last step we used $c_2 = \pi/(\eta T_{p2})$, $k_3 = (1 + \alpha_2) 2^{-1+\frac{3}{2}\eta} \lambda_{\max}(\mathbf{J})^{1-\eta/2}$, $k_4 = 2^{-1-\frac{\eta}{2}} \lambda_{\max}(\mathbf{J})^{1+\eta/2}$, and the fact that $\|\mathbf{s}\|^2 \leq 2V_2/\lambda_{\min}(\mathbf{J}) \leq 2V_2$ (since $\lambda_{\min}(\mathbf{J}) \leq 1$ w.l.o.g. or absorb constants into gain design).

Combining both terms, we obtain

$$\dot{V}_2 \leq \delta_2 V_2^{1/2} - \frac{\pi}{\eta T_{p2}} \left[(1 + \alpha_2) V_2^{1-\frac{\eta}{2}} + V_2^{1+\frac{\eta}{2}} \right], \tag{42}$$

which satisfies the condition of Theorem 1. Hence, $V_2(t)$ converges to the set $V_2 \leq \frac{1}{2}\varepsilon_{\delta_2}^2$ in finite time and remains therein. Since $\|\mathbf{s}\| \leq \sqrt{2V_2/\lambda_{\min}(\mathbf{J})} \leq \sqrt{2}\sqrt{V_2}$, it follows that $\|\mathbf{s}(t)\| \leq \varepsilon_{\delta_2}$. Moreover, the regularization ensures that the set $\{\|\mathbf{s}\| \leq \varepsilon_2\}$ is positively invariant. Combining both cases yields the stated bound $\|\mathbf{s}(t)\| \leq \max\{\varepsilon_{\delta_2}, \varepsilon_2\}$. \square

Remark 5. By selecting an appropriate value of $\alpha_2 > 0$ in conjunction with ε_2 , the designer can ensure $\varepsilon_{\delta_2} \leq \varepsilon_2$, so that the ultimate bound on the sliding surface is governed by the user-specified tolerance ε_2 . This avoids unnecessarily large control gains while achieving the desired steady-state tracking precision.

Remark 6. The inner-loop convergence occurs in two stages. First, Theorem 3 guarantees that $\|\mathbf{s}(t)\| \leq \max\{\varepsilon_{\delta_2}, \varepsilon_2\}$ for all $t \geq T_{p2}$. Set $s_{\max} := \max\{\varepsilon_{\delta_2}, \varepsilon_2\}$. Then Theorem 2 implies that $\boldsymbol{\sigma}_e(t)$ enters $\|\boldsymbol{\sigma}_e\| \leq \max\{\varepsilon_{\delta_1}, \varepsilon_1\}$ for all $t \geq T_{p2} + T_{p1}$. Therefore, it suffices to require $T_{p1} + T_{p2} < T_f$ to ensure the tracking errors settle before the terminal time.

The computable feedforward term $\mathbf{f}(t)$ in (9) can be decomposed as

$$\mathbf{f}(t) = \boldsymbol{\tau}_{\text{ref}}(t) + \Delta_f(t), \tag{43}$$

where $\Delta_f(t) := \mathbf{f}(t) - \boldsymbol{\tau}_{\text{ref}}(t)$ and its component-wise bound is given in Appendix B. The planner enforces $|\tau_{\text{ref},i}(t)| \leq (1 - \gamma_u)\tau_{i,\max}$ on $[0, T_f]$.

Theorem 4. Consider the inner-loop control law (33). Assume that along the closed-loop trajectory over $[0, T_f]$ the tracking errors remain inside the prescribed-accuracy tube, namely, $\|\boldsymbol{\sigma}_e(t)\| \leq \varepsilon_1$, $\|\mathbf{s}(t)\| \leq \varepsilon_2$ for all $t \in [0, T_f]$.

If the safety margin γ_u and prescribed-accuracy set $(\varepsilon_1, \varepsilon_2)$ are selected such that

$$\Delta_{f,i,\max}(\varepsilon_1, \varepsilon_2) + \overline{(J\dot{Q})}_i(\varepsilon_1, \varepsilon_2) + \bar{\tau}_c(\varepsilon_2) \leq \gamma_u \tau_{i,\max}, \quad i = 1, 2, 3, \quad (44)$$

where $\Delta_{f,i,\max}(\varepsilon_1, \varepsilon_2)$, $\overline{(J\dot{Q})}_i(\varepsilon_1, \varepsilon_2)$, and $\bar{\tau}_c(\varepsilon_2)$ are explicit bounds derived in the proof. Then the actuator torques satisfy $|\tau_i(t)| \leq \tau_{i,\max}$ for all $t \in [0, T_f]$ and all $i = 1, 2, 3$.

Proof. By the tube assumption, $\|\sigma_e(t)\| \leq \varepsilon_1$ and $\|s(t)\| \leq \varepsilon_2$ for all $t \in [0, T_f]$. From $s = \omega_e + Q(\sigma_e)$, it follows that

$$\|\omega_e(t)\| \leq \varepsilon_2 + \bar{Q} \quad (45)$$

where \bar{Q} is given in (46).

$$\bar{Q} := \sup_{\|\sigma_e\| \leq \varepsilon_1} \|Q(\sigma_e)\| \leq c_1 \left(k_1 2^{-\eta} \varepsilon_1^{1-\eta} + k_2 2^\eta \varepsilon_1^{1+\eta} \right). \quad (46)$$

From (33) and (43), for each axis i ,

$$|\tau_i| \leq |\tau_{\text{ref},i}| + |\Delta_{f,i}| + |(J\dot{Q})_i| + |\tau_{c,i}|. \quad (47)$$

By the planner tightening, $|\tau_{\text{ref},i}| \leq (1 - \gamma_u) \tau_{i,\max}$.

(i) *Bound on $|\Delta_{f,i}|$.* Appendix B yields, for $i = 1, 2, 3$,

$$|\Delta_{f,i}(t)| \leq (\|\omega_e(t)\| + \|\omega_d(t)\|) H_{\max} + \mu_i \|\omega_e(t)\| \|\omega_d(t)\| + 4\mu_i \|\sigma_e(t)\| \|\dot{\omega}_d(t)\|, \quad (48)$$

where $\mu_i := \sum_{j=1}^3 |J_{ij}|$ and H_{\max} is given in Assumption 3. Using (46) and (12), we obtain

$$|\Delta_{f,i}(t)| \leq \Delta_{f,i,\max}(\varepsilon_1, \varepsilon_2), \quad (49)$$

with

$$\Delta_{f,i,\max}(\varepsilon_1, \varepsilon_2) := (\varepsilon_2 + \bar{Q} + \omega_{d,\max}) H_{\max} + \mu_i (\varepsilon_2 + \bar{Q}) \omega_{d,\max} + 4\mu_i \varepsilon_1 \dot{\omega}_{d,\max}. \quad (50)$$

(ii) *Bound on $|\tau_{c,i}|$.* Since $\|s(t)\| \leq \varepsilon_2$,

$$|\tau_{c,i}(t)| \leq \bar{\tau}_c(\varepsilon_2), \quad \bar{\tau}_c(\varepsilon_2) := c_2 \left(k_3 2^{-\eta} \varepsilon_2^{1-\eta} + k_4 2^\eta \varepsilon_2^{1+\eta} \right). \quad (51)$$

(iii) *Bound on $|(J\dot{Q})_i|$.* By $\dot{Q} = \frac{\partial Q}{\partial \sigma_e} G(\sigma_e) \omega_e$ and (10),

$$\|\dot{Q}(t)\| \leq \left\| \frac{\partial Q}{\partial \sigma_e} \right\| \frac{1 + \varepsilon_1^2}{4} (\varepsilon_2 + \bar{Q}).$$

Moreover, for $\rho := \|\sigma_e\| \leq \varepsilon_1$, a convenient Jacobian envelope is

$$\left\| \frac{\partial Q}{\partial \sigma_e} \right\| \leq \Psi(\varepsilon_1), \quad \Psi(\rho) := c_1 \left[k_1(\rho + \varepsilon_1)^{-\eta} + k_2(\rho + \varepsilon_1)^\eta + \rho(k_1\eta(\rho + \varepsilon_1)^{-\eta-1} + k_2\eta(\rho + \varepsilon_1)^{\eta-1}) \right]. \quad (52)$$

Let $\mu_i := \sum_{j=1}^3 |J_{ij}|$, then $|(Jv)_i| \leq \mu_i \|v\|$, and hence

$$|(J\dot{Q}(t))_i| \leq \overline{(J\dot{Q})}_i(\varepsilon_1, \varepsilon_2), \quad \overline{(J\dot{Q})}_i := \mu_i \Psi(\varepsilon_1) \frac{1 + \varepsilon_1^2}{4} (\varepsilon_2 + \bar{Q}). \quad (53)$$

Finally, substituting the bounds (i)–(iii) into (47) yields

$$|\tau_i(t)| \leq (1 - \gamma_u) \tau_{i,\max} + \Delta_{f,i,\max}(\varepsilon_1, \varepsilon_2) + \overline{(J\dot{Q})}_i(\varepsilon_1, \varepsilon_2) + \bar{\tau}_c(\varepsilon_2).$$

Thus, if (44) holds, then $|\tau_i(t)| \leq \tau_{i,\max}$ for all $t \in [0, T_f]$ and all i . \square

Theorem 5. *Consider the inner-loop control law (33). Assume that along the closed-loop trajectory over $[0, T_f]$ the tracking errors remain inside the prescribed-accuracy tube, namely, $\|\sigma_e(t)\| \leq \varepsilon_1$, $\|s(t)\| \leq \varepsilon_2$ for all $t \in [0, T_f]$.*

If the safety margin γ_h and prescribed-accuracy set $(\varepsilon_1, \varepsilon_2)$ are selected such that

$$H_{\max} + \mu_i(\varepsilon_2 + \bar{Q}) \leq \gamma_h h_{w,i,\max}, \quad i = 1, 2, 3, \quad (54)$$

where \bar{Q} is defined in (46) and $\mu_i := \sum_{j=1}^3 |J_{ij}|$, then the wheel angular momenta satisfy $|h_{w,i}(t)| \leq h_{w,i,\max}$ for all $t \in [0, T_f]$ and all $i = 1, 2, 3$.

Proof. By the tube assumption, the angular-velocity tracking error $\|\omega_e\|$ satisfies (45) for all $t \in [0, T_f]$.

From $\mathbf{h}_w = \mathbf{H} - \mathbf{J}\omega$ and the reference momentum $\mathbf{h}_{w,d} = \mathbf{H}_0 - \mathbf{J}\omega_d$, the actual wheel momentum can be written as

$$\mathbf{h}_w = \mathbf{h}_{w,d} + (\mathbf{H} - \mathbf{H}_0) - \mathbf{J}\omega_e.$$

Taking norms and applying the triangle inequality yields, for each axis i ,

$$\begin{aligned} |h_{w,i}| &\leq |h_{w,d,i}| + \|\mathbf{H} - \mathbf{H}_0\| + \mu_i(\varepsilon_2 + \bar{Q}) \\ &\leq (1 - \gamma_h)h_{w,i,\max} + H_{\max} + \mu_i(\varepsilon_2 + \bar{Q}) \end{aligned} \quad (55)$$

where we used the OCP constraint $|h_{w,d,i}| \leq (1 - \gamma_h)h_{w,i,\max}$ and Assumption 3.

Under condition (54), the right-hand side is bounded by $h_{w,i,\max}$, which completes the proof. \square

Remark 7. *The closed-loop system is initialized on the planned reference trajectory, i.e., $\sigma(0) = \sigma_d(0)$ and $\omega(0) = \omega_d(0)$, hence $\sigma_e(0) = \mathbf{0}$ and $s(0) = \mathbf{0}$. By Theorems 2–3, the regularized neighborhoods $\{\|s\| \leq \varepsilon_2\}$ and $\{\|\sigma_e\| \leq \varepsilon_1\}$ are forward invariant; once entered, the trajectories do not leave. Therefore, in this paper the condition in Theorem 4 and Theorem 5 holds over $[0, T_f]$.*

C. Overall Design Procedure of the EPTPAC Framework

This subsection summarizes a mission-driven synthesis procedure for the proposed EPTPAC framework.

- 1) **Mission inputs and physical limits.** Specify the terminal time $T_f > 0$ and the mission accuracy requirement $\varepsilon_{\text{mission}} > 0$. The inertia \mathbf{J} , wheel limits $\tau_{\max}, h_{w,\max}$, and disturbance bound d_{\max} (Assumption 2) are known.
- 2) **Margins and feasibility.** Choose tightening margins $\gamma_u, \gamma_h \in (0, 1)$ to reserve actuation headroom, e.g. $\gamma_u \gtrsim 2d_{\max}/u_{\max}$ (similarly for γ_h). Verify $T_f \geq T_{f,\min}$ (Assumption 1) via time-optimal analysis or a numerical feasibility test.
- 3) **Accuracy/time allocation and ε_2 scaling.** Set $\varepsilon_1 := \varepsilon_{\text{mission}}$, pick $\eta \in (0, 1)$, and allocate $T_{p1}, T_{p2} > 0$ such that $T_{p1} + T_{p2} < T_f$. Since the sliding surface is $s = \omega_e + \mathbf{Q}(\sigma_e)$ and $\|\mathbf{Q}\| = O(\|\sigma_e\|^{1-\eta})$, set

$$\varepsilon_2 = c \varepsilon_1^{1-\eta}, \quad c > 0. \quad (56)$$

- 4) **Gain selection.** Choose $\alpha_1, \alpha_2 > 0$ such that $\varepsilon_{\delta_1} \leq \varepsilon_1$ and $\varepsilon_{\delta_2} \leq \varepsilon_2$ in Theorems 2–3. With $s_{\max} = \varepsilon_2$ and $\delta_2 = d_{\max}\sqrt{2/\lambda_{\min}(\mathbf{J})}$, sufficient lower bounds are

$$\alpha_1 \geq \alpha_{1,\min} := \frac{\eta T_{p1}}{\pi} 2^{-\eta/2} \frac{\varepsilon_2}{\varepsilon_1^{1-\eta}}, \quad \alpha_2 \geq \alpha_{2,\min} := \frac{\delta_2 \eta T_{p2}}{\pi} \left(\frac{\sqrt{2}}{\varepsilon_2} \right)^{1-\eta}. \quad (57)$$

- 5) **Verify saturation feasibility.** Using the planned reference and the resulting ε_σ from Step 3, verify the sufficient non-saturation condition in Theorem 4. If violated, increase T_f (or T_{p1}, T_{p2}), relax ε_1 , or replan with larger margins γ_u, γ_h and/or a smoother reference.

It is worth noting that the proposed synthesis is not tuning-intensive. In practice, the only parameter that typically

requires adjustment is the exponent η , which mainly trades off smoothness and transient aggressiveness. The remaining quantities are either specified by the mission and hardware ($T_f, \varepsilon_{\text{mission}}, u_{\max}, h_{w,\max}, d_{\max}, J$) or chosen as conservative robustness margins ($\gamma_u, \gamma_h, \kappa$). Once these are set, the rest of the controller parameters (including ε_2 and α_1, α_2) follow automatically from the closed-form rules above.

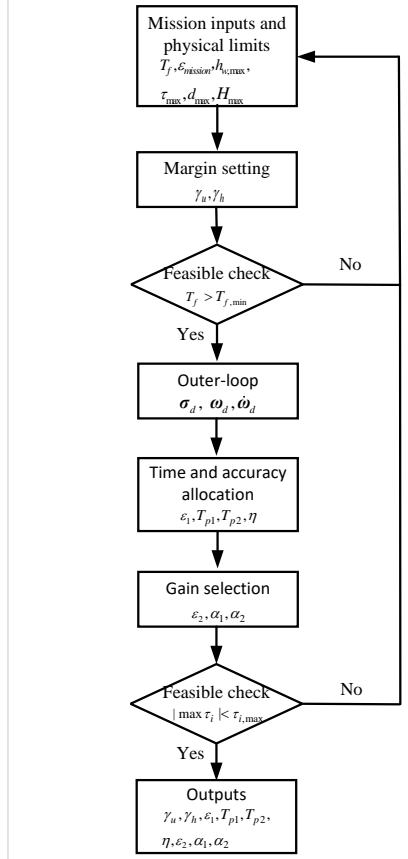


Fig. 2 overall design procedure of the EPTPAC framework.

Remark 8 (Recommended balanced synthesis). *While (56) provides a physically meaningful scaling between ε_2 and ε_1 , the constant c may be selected automatically to avoid unbalanced gains. A convenient choice is to enforce $\alpha_1 = \alpha_2 = \kappa \alpha$ with a safety factor $\kappa > 1$, and determine ε_2 and α by solving $\alpha_{1,\min} = \alpha_{2,\min}$ in (57). This yields*

$$\varepsilon_2 = \left(\frac{\delta_2 \eta T_{p2}}{\eta T_{p1}} 2^{1/2} \right)^{\frac{1}{2-\eta}} \varepsilon_1^{\frac{1-\eta}{2-\eta}}, \quad \alpha = \frac{\eta T_{p1}}{\pi} 2^{-\eta/2} \frac{\varepsilon_2}{\varepsilon_1^{1-\eta}}, \quad (58)$$

followed by $\alpha_1 = \alpha_2 = \kappa \alpha$. This balanced rule yields a unique and reproducible parameter set from mission inputs and physical limits.

IV. Simulation Results

Numerical simulations validate the proposed EPTPAC framework under dual reaction-wheel saturation. Table 2 summarizes the spacecraft parameters, actuator limits, disturbance model, and boundary conditions. Theoretical guarantees apply over the mission interval $[0, T_f]$. The simulation horizon is extended to $T_{\text{sim}} > T_f$ to observe post-maneuver behavior, with the reference held constant at the target state for $t \geq T_f$.

Table 2 Common simulation settings and boundary conditions

Symbol	Value
\mathbf{J}	$\text{diag}([200, 250, 300]) \text{ kg} \cdot \text{m}^2$
$\tau_{i,\text{max}}$	$0.2 \text{ N} \cdot \text{m}$
$h_{w,i,\text{max}}$	$4.0 \text{ kg} \cdot \text{m}^2/\text{s}$
$\mathbf{d}(t)$	$0.01 [\sin(2t), \cos(t), \cos(t+2)]^\top \text{ N} \cdot \text{m}$
d_{max}	$\sqrt{3} \times 0.01 \text{ N} \cdot \text{m}$
$\sigma(0)$	$[0.2, 0.3, -0.3]^\top$
σ_{target}	$[0, 0, 0]^\top$
$\omega(0)$	$[0, 0, 0]^\top \text{ rad/s}$
ω_{target}	$[0, 0, 0]^\top \text{ rad/s}$
$\mathbf{h}_w(0)$	$[0, 0, 0]^\top \text{ kg} \cdot \text{m}^2/\text{s}$

The outer-loop reference (σ_d, ω_d) is generated offline by solving the constrained OCP (22) using GPOPS-II with $\lambda = 0.1$ and $N = 20$ nodes. The nodal torques are converted to a continuous-time command via piecewise-linear interpolation (23).

Four comprehensive cases are studied to validate different aspects of the framework: Case 1 validates baseline performance with dual-constraint compliance; Case 2 assesses exact terminal-time convergence across different T_f ; Case 3 demonstrates accuracy tunability; and Case 4 compares against an existing prescribed-time controller.

A. Case 1: Baseline Maneuver

This case validates the baseline performance of the EPTPAC framework, demonstrating exact terminal-time convergence and strict compliance with dual actuator constraints. The terminal time is set to $T_f = 120 \text{ s}$ with mission-level attitude accuracy $\varepsilon_1 = 10^{-5}$. The inner-loop convergence times are allocated as $T_{p2} = 15 \text{ s}$ and $T_{p1} = 100 \text{ s}$, ensuring $T_{p1} + T_{p2} = 115 \text{ s} < T_f$ to provide temporal margin. Design parameters include the prescribed-time exponent $\eta = 0.2$ and safety margins $\gamma_u = \gamma_h = 0.1$ for actuator headroom.

Following the synthesis procedure in Section III.C with balancing factor $\kappa = 1.2$, the inner-loop parameters are computed as $\varepsilon_2 = 8.0213 \times 10^{-5}$ and $\alpha_1 = \alpha_2 = 5.7174$. The practical convergence bounds from Theorems 2–3 are $\varepsilon_{\delta_1} = 7.9620 \times 10^{-6}$ and $\varepsilon_{\delta_2} = 6.3865 \times 10^{-5}$, both satisfying $\varepsilon_{\delta_i} < \varepsilon_i$. Thus, the ultimate tracking accuracy is governed by the user-specified tolerances $(\varepsilon_1, \varepsilon_2)$.

Figure 3 illustrates the reference tracking performance. The spacecraft attitude in MRPs and angular velocity closely follows the planned trajectory, with the reference reaching the target state exactly at $t = T_f$ by construction.

Figure 4 displays the error convergence profiles. Due to consistent initialization ($\sigma(0) = \sigma_d(0)$, $\omega(0) = \omega_d(0)$), all tracking errors start at zero and remain within prescribed neighborhoods throughout the maneuver.

Figure 5 demonstrates physical realizability under dual saturation. Both torque components and wheel momentum remain strictly within their prescribed limits throughout $[0, T_f]$, validating the constraint-aware trajectory planning and bounded inner-loop corrections.

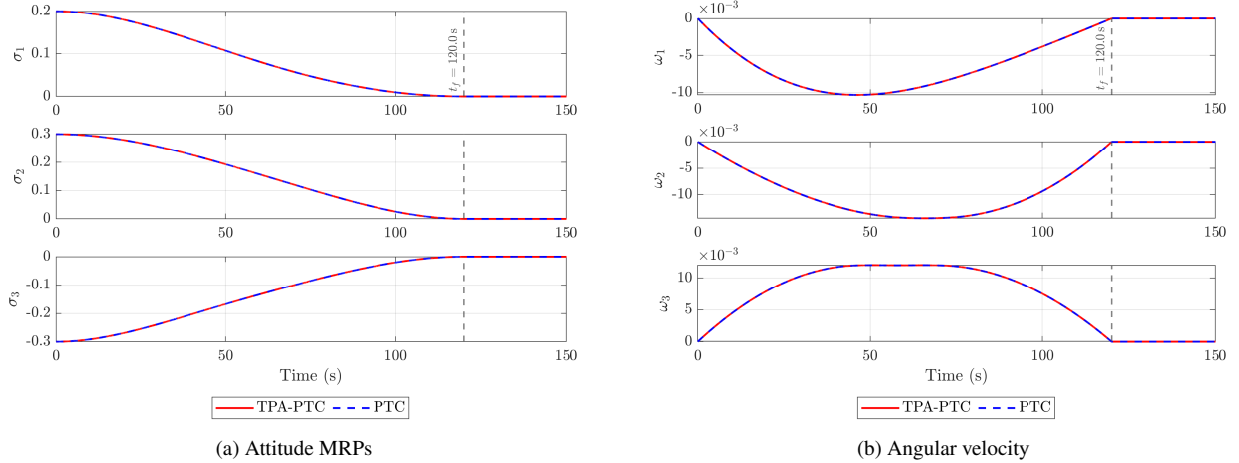


Fig. 3 Case 1: Reference tracking in MRPs and angular rates.

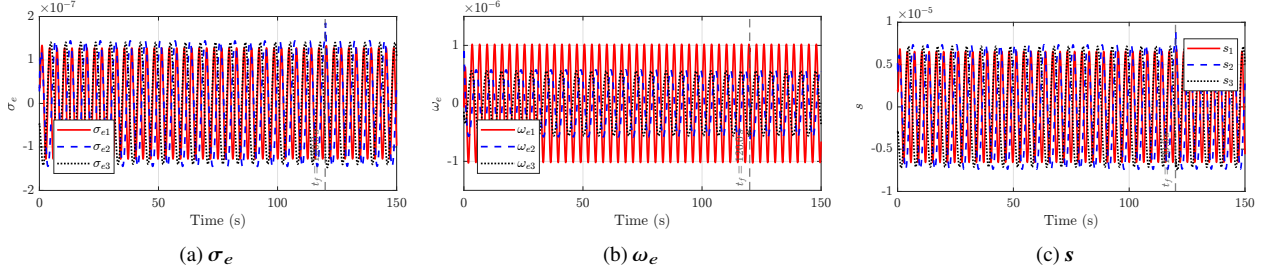


Fig. 4 Case 1: Errors responses

To assess robustness against beyond-bound transient perturbations, a severe disturbance injection is applied during the first second:

$$\mathbf{d}(t) = \begin{cases} 0.05 [1, 1, 1]^\top \text{ N} \cdot \text{m}, & 0 \leq t < 1, \\ \mathbf{d}_{\text{base}}(t), & t \geq 1, \end{cases} \quad (59)$$

where $\mathbf{d}_{\text{base}}(t)$ denotes the nominal bounded disturbance from Table 2. The injected disturbance magnitude $0.05 \text{ N} \cdot \text{m}$ exceeds the design bound $d_{\text{max}} \approx 0.0173 \text{ N} \cdot \text{m}$, potentially driving the trajectory outside the guaranteed practical convergence neighborhoods of Assumption 2.

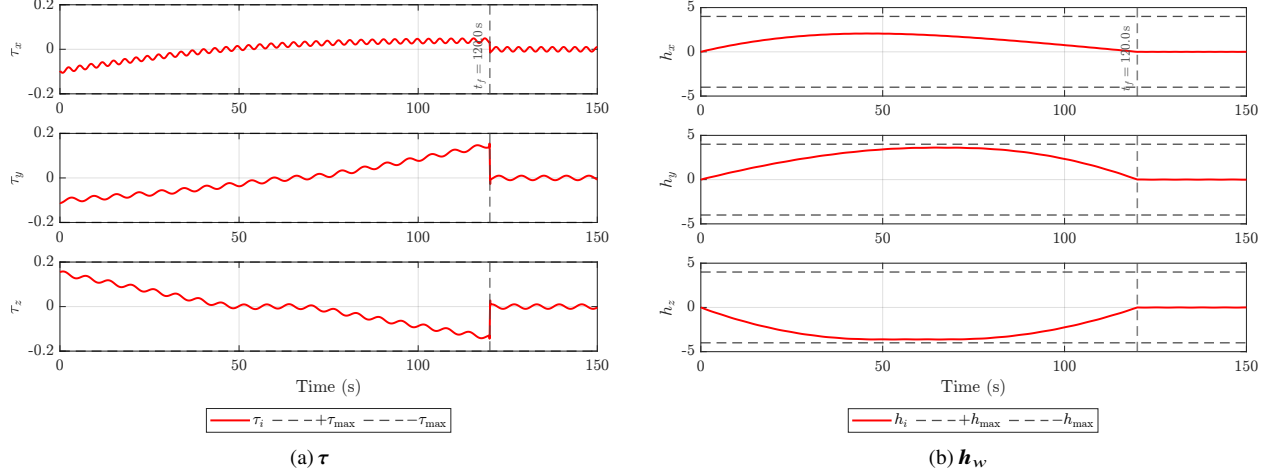


Fig. 5 Case 1: Torque and wheel momentum.

Despite this severe transient, Figs. 6–7 demonstrate robust recovery. Upon disturbance removal at $t = 1$ s, the tracking errors rapidly return to their prescribed neighborhoods within the scheduled convergence times $T_{p1} + T_{p2} = 115$ s.

Critically, both torque and wheel momentum remain strictly within their saturation limits throughout the entire maneuver, including during the disturbance period, validating the framework's robustness margins and constraint-aware design.

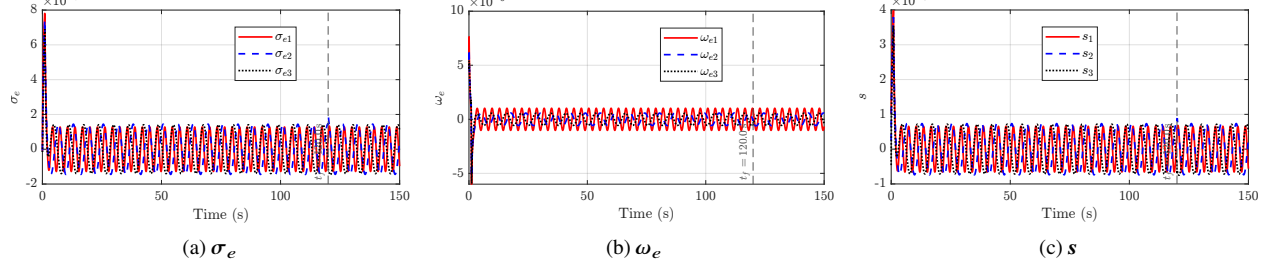


Fig. 6 Case 1: Error convergence under beyond-bound transient disturbance.

This case demonstrates time-anchored convergence with dual-constraint compliance and rapid recovery under beyond-bound disturbances.

B. Case 2: Time-Flexibility Assessment

Before presenting Case 2, we clarify notation. The tracking error σ_e is defined relative to the reference $\sigma_d(t)$. To highlight the prescribed terminal-time tracking relative to the fixed target, we additionally report the target-pointing MRP error $\sigma_{e,\text{tar}}$, defined between the current attitude $\sigma(t)$ and the constant target σ_{target} .

This case verifies that the framework ensures exact terminal-time convergence across different terminal times while maintaining feasibility under dual actuator constraints. For all $T_f \in \{110 \text{ s}, 120 \text{ s}, 130 \text{ s}, 140 \text{ s}\}$, the closed-loop system reaches the target at the commanded time with prescribed tracking accuracy, while control torque and wheel momentum

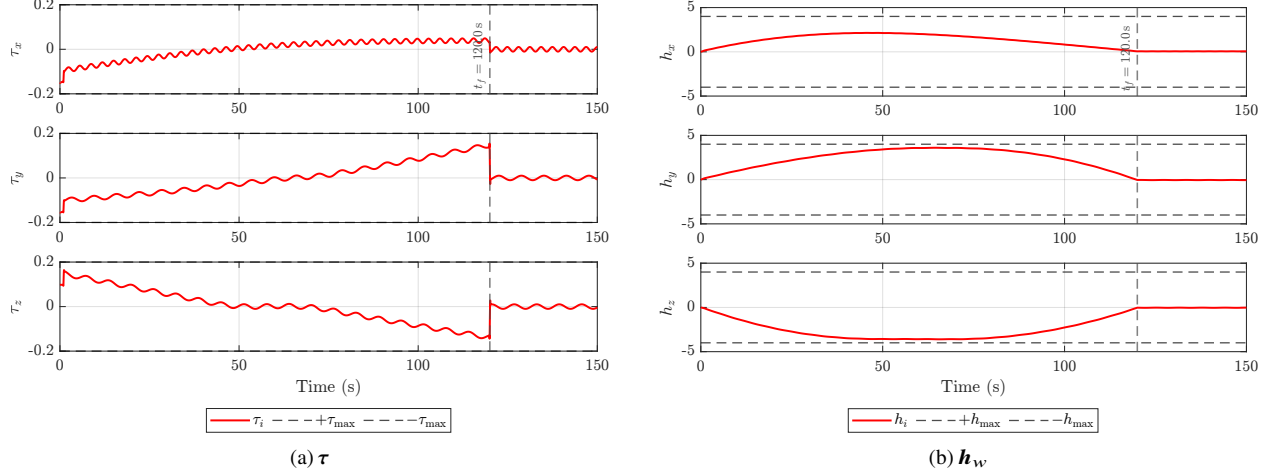


Fig. 7 Case 1: Torque and wheel momentum under the beyond-bound transient disturbance.

remain within limits.

The study uses the same settings as Case 1, with $\varepsilon_1 = 10^{-5}$, $\eta = 0.2$, $\gamma_u = \gamma_h = 0.1$, and time allocation $T_{p2} = 15$ s, $T_{p1} = T_f - 20$ s (so $T_{p1} + T_{p2} = T_f - 5$ s $< T_f$). For each T_f , the outer-loop OCP (22) is solved to generate a dual-constraint-feasible reference, and inner-loop parameters are synthesized using the balanced rule with $\kappa = 1.2$.

Table 3 Case 2: Synthesized parameters for terminal-time sweep

T_f	T_{p1}	T_{p2}	ε_2	$\alpha_1 = \alpha_2$
110 s	90 s	15 s	8.505×10^{-5}	5.456
120 s	100 s	15 s	8.021×10^{-5}	5.717
130 s	110 s	15 s	7.608×10^{-5}	5.965
140 s	120 s	15 s	7.249×10^{-5}	6.200

Figures 8–10 display the responses. Figure 8 shows that the target-pointing error components decay into prescribed neighborhoods before their respective terminal times, confirming exact terminal-time convergence. Figures 9 and 10 reveal the expected trade-off: shorter T_f demands more aggressive actuation with higher torque and faster wheel-momentum accumulation, yet both remain within hardware limits due to constraint-aware planning.

The table 5 reveals that the actual convergence time is marginally earlier than the prescribed terminal time T_f , with a discrepancy of approximately 0.2–0.3 seconds. This early entry is attributed to the conservative design of the accuracy tolerance $\varepsilon_1 = 10^{-5}$, which ensures robust performance margins under disturbances and modeling errors. Since the early arrival is minimal and the tracking error remains well within the prescribed accuracy bound, the framework successfully achieves practical exact-time convergence while maintaining safety margins in the presence of uncertainties.

In summary, Case 2 confirms that the proposed framework provides a practical interface to schedule the maneuver at user-specified terminal times. By re-planning the dual-constraint-feasible reference on $[0, T_f]$ and re-synthesizing

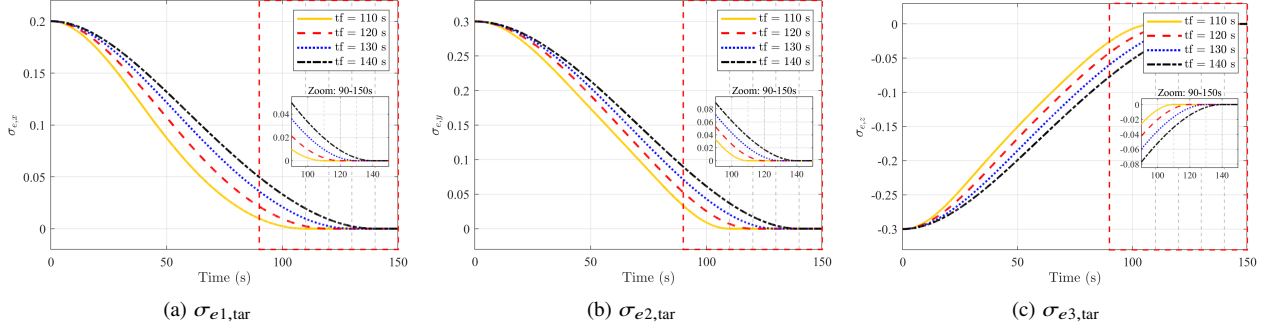


Fig. 8 Case 2: MRP error components for different T_f

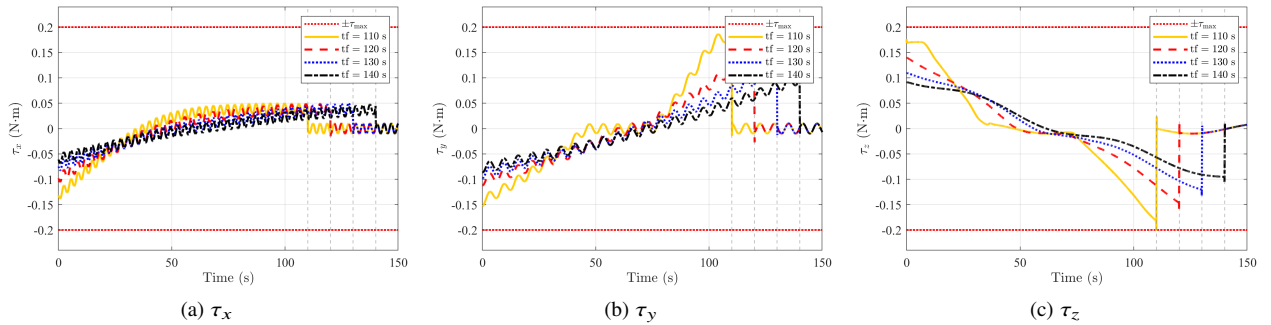


Fig. 9 Case 2: Control torque components for different T_f

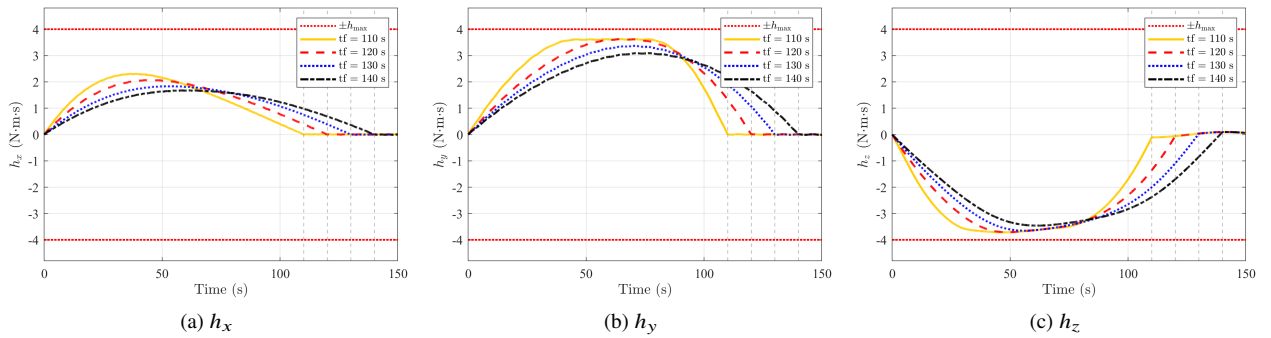


Fig. 10 Case 2: Wheel momentum components for different T_f

the tracking parameters accordingly, the closed-loop system ensures exact terminal-time convergence across a wide range of T_f values. The results also reveal the expected trade-off: shorter T_f leads to higher torque demand and faster wheel-momentum accumulation, while all runs remain realizable under the prescribed actuator limits due to the constraint-aware co-design.

C. Case 3: Precision-sweep assessment under identical conditions

This case demonstrates prescribed-accuracy tunability under the same operating condition as Case 1, with the terminal time fixed at $T_f = 120$ s. Set $\eta = 0.2$, $\gamma_u = \gamma_h = 0.1$, $T_{p2} = 15$ s, and $T_{p1} = 100$ s, and sweep the prescribed attitude tolerance as $\varepsilon_1 \in \{10^{-4}, 10^{-5}, 10^{-6}, 10^{-7}\}$. For each ε_1 , the remaining inner-loop parameters are synthesized using the balanced rule in Section III.C with $\kappa = 1.2$, producing $(\varepsilon_2, \alpha_1, \alpha_2)$ together with the practical bounds $(\varepsilon_{\delta_1}, \varepsilon_{\delta_2})$ from Theorems 2–3. The resulting values are reported in Table 4.

Table 4 Case 3: Synthesized parameters for accuracy sweep

ε_1	ε_2	$\alpha_1 = \alpha_2$	ε_{δ_1}	ε_{δ_2}
1×10^{-4}	2.232×10^{-4}	2.521	7.962×10^{-5}	1.777×10^{-4}
1×10^{-5}	8.021×10^{-5}	5.717	7.962×10^{-6}	6.387×10^{-5}
1×10^{-6}	2.883×10^{-5}	12.965	7.962×10^{-7}	2.295×10^{-5}
1×10^{-7}	1.036×10^{-5}	29.398	7.962×10^{-8}	8.249×10^{-6}

The log-scale responses in Fig. 11 show that all runs achieve their prescribed accuracy: $\|\sigma_e(t)\|$ decreases below the threshold ε_1 and remains therein, while $\|s(t)\|$ is regulated below ε_2 . This confirms the framework provides a direct interface for tuning mission accuracy through ε_1 .

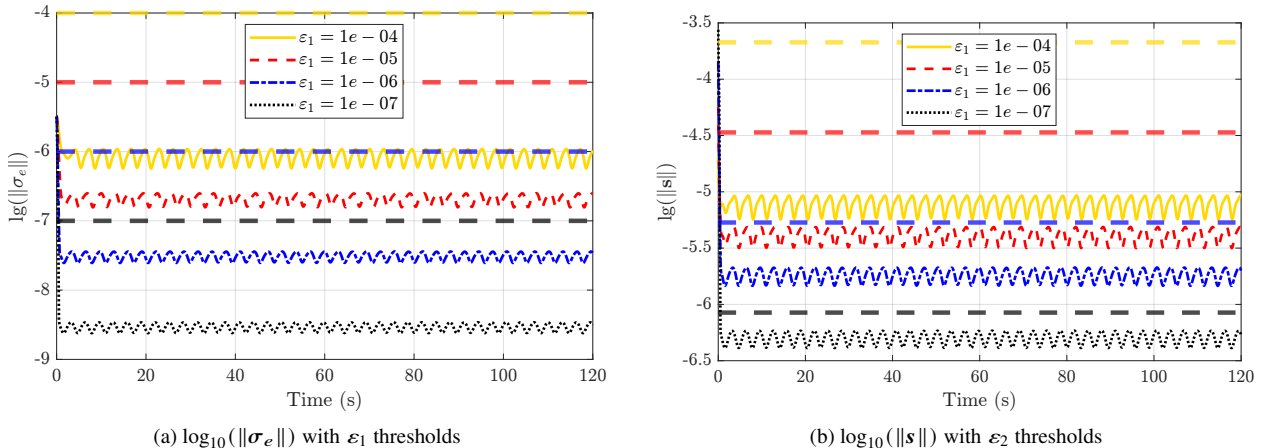


Fig. 11 Case 3: Log-scale comparison of $\|\sigma_e\|$ and $\|s\|$ for different ε_1

As ε_1 tightens from 10^{-4} to 10^{-7} , the achieved accuracy decreases and induced sliding tolerance ε_2 also decreases. Correspondingly, gains α_1 and α_2 increase substantially (Table 4), raising control activity. In practice, ε_1 should be

selected to match sensor accuracy and actuation resources; pursuing excessively tight tolerances is unnecessary and may degrade robustness margins.

Table 5 Case 2: First entry time of $\|\sigma_{e,\text{tar}}\|$ into prescribed accuracy neighborhoods

T_f (s)	First entry into 10^{-5} (s)	First entry into 10^{-6} (s)
110	109.75	109.94
120	119.76	119.93
130	129.75	129.94
140	139.75	139.94

In summary, Case 3 confirms that the framework systematically enforces prescribed accuracy levels through ε_1 . Tightening ε_1 reduces tracking residual but requires larger gains and higher control effort. Thus, ε_1 should be selected based on achievable sensing accuracy and actuation margins.

D. Case 4: Comparison with Existing Prescribed-Time Saturated Control

To demonstrate the superiority of the proposed framework, Case 4 compares against a representative predefined-time saturated controller from [15]. Two scenarios evaluate prescribed terminal-time tracking performance and robustness to dual saturation.

1. Case 4.1: Prescribed terminal-time tracking under varying margins

This scenario evaluates prescribed terminal-time tracking under two commands: an ample-margin case ($T_f = 300$ s) and a tight-margin case ($T_f = 150$ s). Only torque saturation ($\tau_{i,\text{max}} = 0.2$ N · m) is enforced. Results are shown in Fig. 12.

For the ample-margin case ($T_f = 300$ s), Figs. 12a and 12b reveal that the baseline exhibits significant conservatism: tracking error converges around 150 s, far earlier than the prescribed 300 s. This premature convergence induces unnecessary control effort and wastes momentum resources—undesirable for long-duration missions or synchronized operations.

For the tight-margin case ($T_f = 150$ s), the baseline’s limitations become acute. As shown in Figs. 12c and 12d, high-gain feedback combined with torque limits destroys the nominal prescribed-time behavior. The spacecraft fails to arrive within 150 seconds, with convergence delayed to approximately 230 seconds.

In contrast, EPTPAC ensures convergence exactly at the prescribed times with smooth, optimized profiles. This comparison demonstrates that existing prescribed-time methods, while theoretically sound without constraints, fail to maintain reliable prescribed terminal-time tracking when saturations are enforced. EPTPAC resolves this by embedding physical limits into the planning layer.

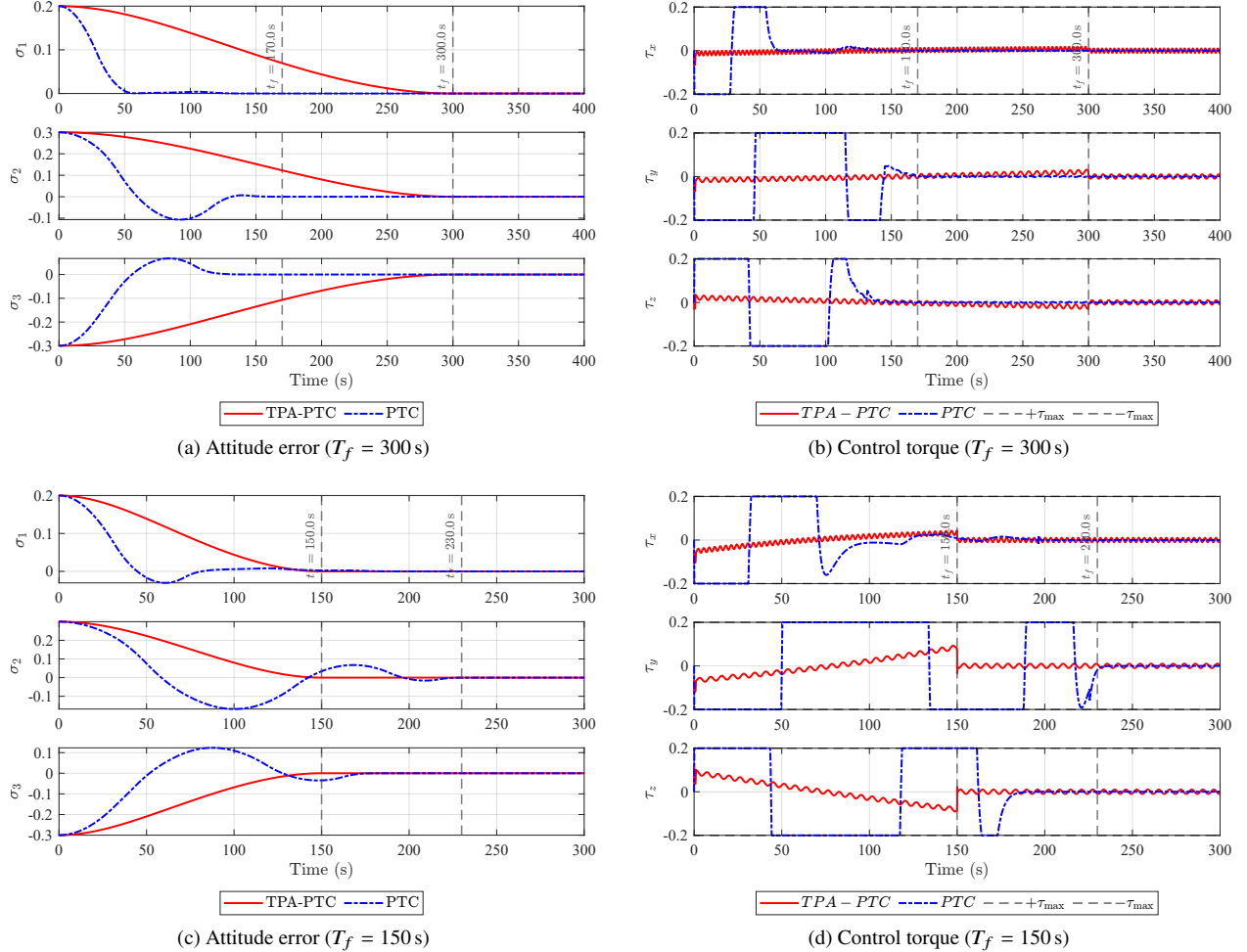


Fig. 12 Case 4.1: Performance comparison under torque-only saturation.

2. Case 4.2: Dual saturation (torque and wheel momentum)

This scenario evaluates robustness under stringent dual saturation constraints with $T_f = 300$ s. Results are shown in Fig. 13.

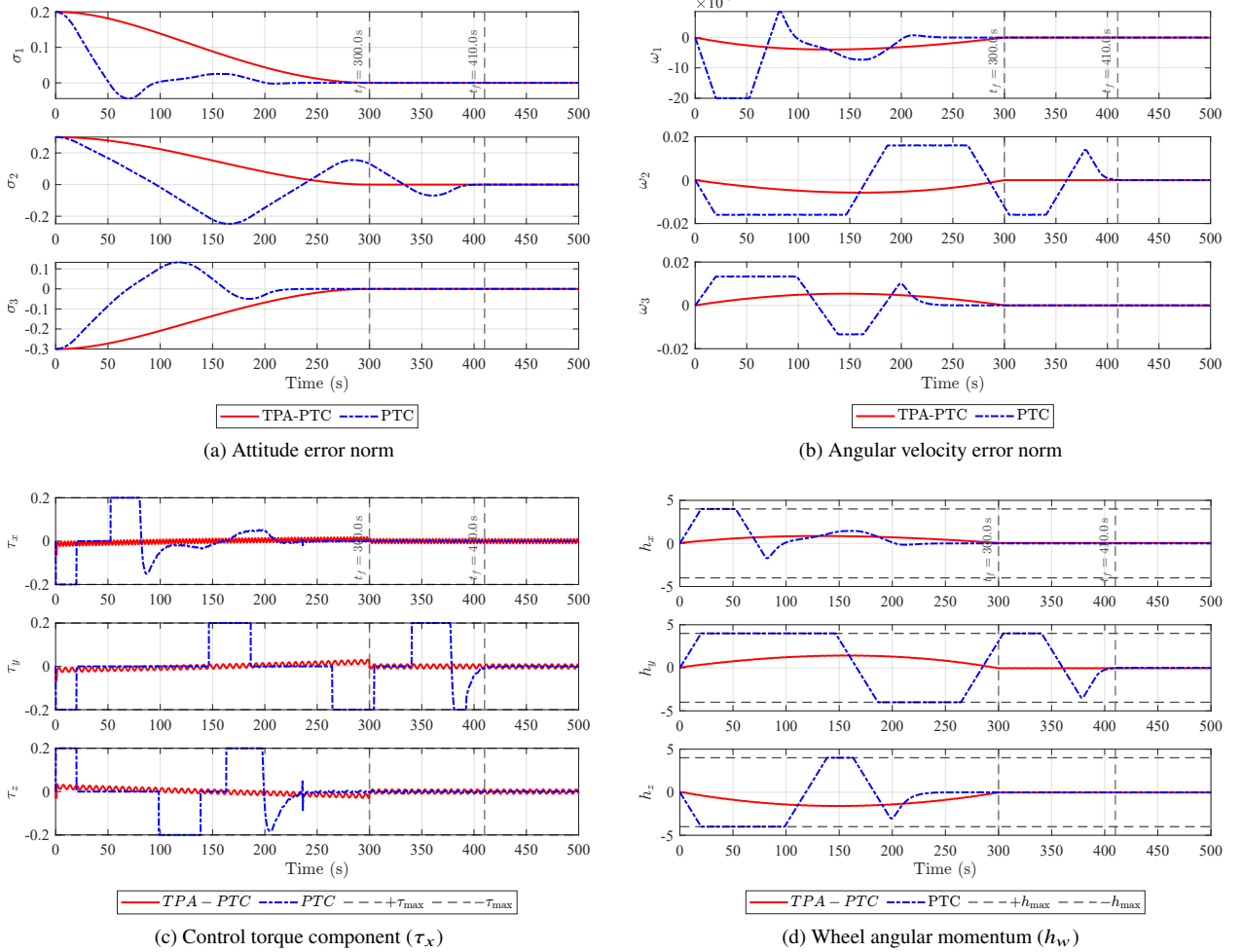


Fig. 13 Case 4.2: Performance comparison under dual saturation

The simulation results reveal a significant performance gap between the two frameworks under dual saturation. As shown in Fig. 13(d), the baseline controller, lacking a predictive awareness of momentum storage, demands excessive control effort early in the maneuver. This causes the wheel momentum to hit its hard ceiling of $4.0 \text{ kg} \cdot \text{m}^2/\text{s}$ at approximately $t = 120$ s, effectively stripping the spacecraft of its control authority. During this saturation interval, the control torque is forced to zero or remains ineffective (Fig. 13(c)), leading to the uncontrolled "drift" observed in the attitude and angular velocity errors (Figs. 13(a) and (b)). Consequently, the baseline's convergence is delayed to 410 s, far exceeding the 300-second requirement.

In contrast, the EPTPAC framework successfully navigates these mission-critical constraints. The outer-loop

trajectory planner generates a reference that strategically allocates torque to prevent the wheels from ever reaching the momentum ceiling. As a result, the inner-loop tracking errors remain small and well-behaved throughout the mission window. By tracking this constraint-feasible reference, the spacecraft reaches the target state with the prescribed accuracy exactly at $t = 300$ s. This outcome demonstrates that the integration of optimal planning and prescribed-time control is indispensable for ensuring the physical realizability of timed maneuvers in the presence of complex dual-saturation effects.

In summary, Case 4 shows that enforcing actuator saturation can destroy the nominal terminal-time behavior of predefined-time controllers derived under unconstrained assumptions, whereas EPTPAC ensures exact terminal-time convergence by co-designing a saturation-feasible reference and a bounded prescribed-time tracker.

V. Conclusion

This paper proposed a EPTPAC framework for reaction-wheel spacecraft that must reach a commanded attitude *exactly* at a user-specified terminal time while strictly satisfying both torque and wheel momentum limits. The approach combines a constraint-aware, time-anchored trajectory planner with a nonsingular prescribed-time tracking controller, yielding explicit practical prescribed-time accuracy bounds and a sufficient feasibility condition that relates actuator limits, margins, prescribed-time parameters, and admissible initial errors.

Simulation results demonstrated exact-time arrival with guaranteed constraint satisfaction under significant disturbances, consistent performance across multiple prescribed terminal times, and predictable accuracy changes under a precision sweep. Comparisons with a conventional prescribed-time controller under enforced actuator constraints further illustrated that saturation can destroy the nominal prescribed-time behavior and significantly prolong settling, underscoring the necessity of constraint-aware co-design for physically realizable timed maneuvers.

Future work will investigate reduced-complexity/online planning, robustness to model uncertainty, and integrated momentum-management strategies for long-duration operations.

A. A Bang-Bang Estimate of $T_{f,\min}$

This appendix provides a bang-bang estimate of the minimum feasible maneuver time under component-wise torque and wheel-momentum limits. It is used as a conservative screening rule for selecting T_f in Assumption 1.

Let $\sigma_e(0)$ denote the initial attitude error in MRPs. The associated principal rotation angle $\theta \in [0, \pi]$ and axis $e = [e_1, e_2, e_3]^T$ are

$$\theta = 4 \arctan(\|\sigma_e(0)\|), \quad e = \begin{cases} \frac{\sigma_e(0)}{\|\sigma_e(0)\|}, & \sigma_e(0) \neq \mathbf{0}, \\ \text{any unit vector, } \sigma_e(0) = \mathbf{0}. & \end{cases} \quad (60)$$

Define the effective inertia $J_e := \mathbf{e}^T \mathbf{J} \mathbf{e}$. With $|\tau_i| \leq \tau_{i,\max}$, the maximum torque projection along \mathbf{e} is

$$\tau_{e,\max} = \max_{|\tau_i| \leq \tau_{i,\max}} \mathbf{e}^T \boldsymbol{\tau} = \sum_{i=1}^3 |e_i| \tau_{i,\max}. \quad (61)$$

Assume $\mathbf{h}_w(0) = \mathbf{0}$ and $|h_{w,i}| \leq h_{w,i,\max}$. Under the bang-bang allocation $\tau_i = \text{sgn}(e_i) \tau_{i,\max}$, the maximum duration before wheel-momentum saturation is

$$t_h := \min_{i \in \{1,2,3\}} \frac{h_{w,i,\max}}{\tau_{i,\max}}. \quad (62)$$

For a nominal rest-to-rest rotation about \mathbf{e} , the peak rate and the corresponding no-coast angle are

$$\omega_{\max} = \frac{\tau_{e,\max}}{J_e} t_h, \quad \theta_h = \frac{\tau_{e,\max}}{J_e} t_h^2. \quad (63)$$

The resulting minimum-time estimate is

$$T_{f,\min} \approx \begin{cases} 2\sqrt{\frac{J_e \theta}{\tau_{e,\max}}}, & \theta \leq \theta_h, \\ 2t_h + \frac{\theta - \theta_h}{\omega_{\max}}, & \theta > \theta_h. \end{cases} \quad (64)$$

B. Bound on the feedforward mismatch

Let $\mathbf{H}_d(t) := \mathbf{J}\omega_d(t) + \mathbf{h}_{w,d}(t)$ denote the total angular momentum of the reference trajectory. Since the reference is generated under disturbance-free dynamics and initialized with the same total momentum as the actual spacecraft ($\mathbf{H}_d(0) = \mathbf{H}(0) =: \mathbf{H}_0$), the reference total angular momentum is conserved, i.e.,

$$\mathbf{H}_d(t) \equiv \mathbf{H}_0, \quad \forall t \in [0, T_f].$$

The planned torque is therefore

$$\boldsymbol{\tau}_{\text{ref}}(t) = \mathbf{J}\dot{\omega}_d(t) + \omega_d(t)^{\times} \mathbf{H}_0. \quad (65)$$

The feedforward mismatch is defined as $\Delta_f(t) := \mathbf{f}(t) - \boldsymbol{\tau}_{\text{ref}}(t)$. Substituting $\mathbf{f}(t)$ from (9) yields

$$\Delta_f(t) = -\omega(t)^{\times} \mathbf{H}(t) + \mathbf{J}\omega_e(t)^{\times} \mathbf{R}(\sigma_e(t))\omega_d(t) + \mathbf{J}(\mathbf{R}(\sigma_e(t)) - \mathbf{I})\dot{\omega}_d(t) - \omega_d(t)^{\times} \mathbf{H}_0. \quad (66)$$

Grouping the momentum-dependent terms gives

$$\Delta_f(t) = -\omega(t)^\times(\mathbf{H}(t) - \mathbf{H}_0) - \omega_e(t)^\times\mathbf{H}_0 + \mathbf{J}\omega_e(t)^\times\mathbf{R}(\sigma_e(t))\omega_d(t) + \mathbf{J}(\mathbf{R}(\sigma_e(t)) - \mathbf{I})\dot{\omega}_d(t).$$

From Assumption 3, the momentum drift satisfies

$$\|\mathbf{H}(t) - \mathbf{H}_0\| \leq H_{\max}, \quad \forall t \in [0, T_f]. \quad (67)$$

Using $\|\mathbf{a}^\times\mathbf{b}\| \leq \|\mathbf{a}\|\|\mathbf{b}\|$, $\|\mathbf{R}(\sigma_e)\| = 1$, and $\|\mathbf{R}(\sigma_e) - \mathbf{I}\| \leq 4\|\sigma_e\|$ (valid for $\|\sigma_e\| < 1$), each axis component of $\Delta_f(t)$ satisfies

$$|\Delta_{f,i}(t)| \leq \|\omega(t)\| H_{\max} + \mu_i \|\omega_e(t)\| \|\mathbf{H}_0\| + \mu_i \|\omega_e(t)\| \|\omega_d(t)\| + 4\mu_i \|\sigma_e(t)\| \|\dot{\omega}_d(t)\|, \quad (68)$$

where $\mu_i := \sum_{j=1}^3 |J_{ij}|$. Since $\|\mathbf{H}_0\| = H_0$ and $\|\omega(t)\| \leq \|\omega_e(t)\| + \|\omega_d(t)\|$, we obtain

$$|\Delta_{f,i}(t)| \leq (\|\omega_e(t)\| + \|\omega_d(t)\|) H_{\max} + \mu_i \|\omega_e(t)\| \|\mathbf{H}_0\| + \mu_i \|\omega_e(t)\| \|\omega_d(t)\| + 4\mu_i \|\sigma_e(t)\| \|\dot{\omega}_d(t)\|. \quad (69)$$

Taking the supremum over $[0, T_f]$ and using the bounds $\|\omega_e(t)\| \leq \omega_{e,\max}$, $\|\sigma_e(t)\| \leq \sigma_{\max}$, $\|\omega_d(t)\| \leq \omega_{d,\max}$, $\|\dot{\omega}_d(t)\| \leq \dot{\omega}_{d,\max}$, we obtain the component-wise envelope

$$\Delta_{f,i,\max} := (\omega_{e,\max} + \omega_{d,\max}) H_{\max} + \mu_i \omega_{e,\max} H_0 + \mu_i \omega_{e,\max} \omega_{d,\max} + 4\mu_i \sigma_{\max} \dot{\omega}_{d,\max}, \quad i = 1, 2, 3. \quad (70)$$

References

- [1] Alex Pothen, A., Crain, A., and Ulrich, S., “Pose Tracking Control for Spacecraft Proximity Operations Using the Udwadia–Kalaba Framework,” *Journal of Guidance, Control, and Dynamics*, Vol. 45, No. 2, 2022, pp. 296–309. <https://doi.org/10.2514/1.G005169>, URL <https://doi.org/10.2514/1.G005169>, publisher: American Institute of Aeronautics and Astronautics _eprint: <https://doi.org/10.2514/1.G005169>.
- [2] Sun, H.-J., Wu, Y.-Y., and Zhang, J., “Attitude synchronization control for multiple spacecraft: A preassigned finite-time scheme,” *Advances in Space Research*, Vol. 73, No. 12, 2024, pp. 6094–6110. <https://doi.org/10.1016/j.asr.2024.02.001>, URL <https://www.sciencedirect.com/science/article/pii/S0273117724001303>.
- [3] Xu, C., Zelazo, D., and Wu, B., “Distributed prescribed-time coordinated control of spacecraft formation flying under input saturation,” *Advances in Space Research*, Vol. 74, No. 5, 2024, pp. 2302–2315. <https://doi.org/10.1016/j.asr.2024.05.077>, URL <https://www.sciencedirect.com/science/article/pii/S027311772400543X>.
- [4] Hong, Y., and Jiang, Z.-P., “Finite-Time Stabilization of Nonlinear Systems With Parametric and Dynamic Uncertainties,” *IEEE Transactions on Automatic Control*, Vol. 51, No. 12, 2006, pp. 1950–1956. <https://doi.org/10.1109/TAC.2006.886515>, URL <https://ieeexplore.ieee.org/document/4026648/>.
- [5] Zhou, B., “Finite-time stability analysis and stabilization by bounded linear time-varying feedback,” *Automatica*, Vol. 121, 2020, p. 109191. <https://doi.org/10.1016/j.automatica.2020.109191>, URL <https://www.sciencedirect.com/science/article/pii/S0005109820303897>.
- [6] Polyakov, A., “Nonlinear Feedback Design for Fixed-Time Stabilization of Linear Control Systems,” *IEEE Transactions on Automatic Control*, Vol. 57, No. 8, 2012, pp. 2106–2110. <https://doi.org/10.1109/TAC.2011.2179869>, URL <https://ieeexplore.ieee.org/document/6104367/>.
- [7] Polyakov, A., Efimov, D., and Perruquetti, W., “Finite-time and fixed-time stabilization: Implicit Lyapunov function approach,” *Automatica*, Vol. 51, 2015, pp. 332–340. <https://doi.org/10.1016/j.automatica.2014.10.082>, URL <https://www.sciencedirect.com/science/article/pii/S0005109814004634>.
- [8] Sánchez-Torres, J. D., Sanchez, E. N., and Loukianov, A. G., “Predefined-time stability of dynamical systems with sliding modes,” *2015 American Control Conference (ACC)*, 2015, pp. 5842–5846. <https://doi.org/10.1109/ACC.2015.7172255>, URL <https://ieeexplore.ieee.org/document/7172255>, iSSN: 2378-5861.
- [9] Sánchez-Torres, J. D., Gómez-Gutiérrez, D., López, E., and Loukianov, A. G., “A class of predefined-time stable dynamical systems,” *IMA Journal of Mathematical Control and Information*, Vol. 35, No. Supplement_1, 2018, pp. i1–i29. <https://doi.org/10.1093/imamci/dnx004>, URL <https://doi.org/10.1093/imamci/dnx004>.
- [10] Anguiano-Gijón, C. A., Muñoz-Vázquez, A. J., Sánchez-Torres, J. D., Romero-Galván, G., and Martínez-Reyes, F., “On predefined-time synchronisation of chaotic systems,” *Chaos, Solitons & Fractals*, Vol. 122, 2019, pp. 172–178. <https://doi.org/10.1016/j.chaos.2019.03.015>, URL <https://www.sciencedirect.com/science/article/pii/S0960077919300864>.

- [11] Ye, D., Zou, A.-M., and Sun, Z., “Predefined-Time Predefined-Bounded Attitude Tracking Control for Rigid Spacecraft,” *IEEE Transactions on Aerospace and Electronic Systems*, Vol. 58, No. 1, 2022, pp. 464–472. <https://doi.org/10.1109/TAES.2021.3103258>, URL <https://ieeexplore.ieee.org/abstract/document/9512481>.
- [12] Muñoz-Vázquez, A. J., Sánchez-Torres, J. D., Gutiérrez-Alcalá, S., Jiménez-Rodríguez, E., and Loukianov, A. G., “Predefined-time robust contour tracking of robotic manipulators,” *Journal of the Franklin Institute*, Vol. 356, No. 5, 2019, pp. 2709–2722. <https://doi.org/10.1016/j.jfranklin.2019.01.041>, URL <https://www.sciencedirect.com/science/article/pii/S0016003219300973>.
- [13] Meng, Y., Zhu, Y., Cui, Y., and Qiao, J., “Predefined-Time Enhanced Antidisturbance Attitude Control for Rigid-Liquid Coupled Launch Vehicles,” *Journal of Guidance Control and Dynamics*, Vol. 48, No. 4, 2025, pp. 870–884. <https://doi.org/10.2514/1.G008397>, num Pages: 15 Place: Reston Publisher: Amer Inst Aeronautics Astronautics Web of Science ID: WOS:001403479000001.
- [14] Xiao, Y., Wang, Y., Ye, D., and Sun, Z., “Predefined-time robust attitude tracking control of flexible spacecraft with continuous and nonsingular performance,” *Aerospace Science and Technology*, Vol. 159, 2025, p. 110000. <https://doi.org/10.1016/j.ast.2025.110000>, URL <https://www.sciencedirect.com/science/article/pii/S1270963825000720>.
- [15] Xu, C., Wu, B., and Wang, D., “Distributed Prescribed-Time Attitude Coordination for Multiple Spacecraft With Actuator Saturation Under Directed Graph,” *IEEE Transactions on Aerospace and Electronic Systems*, Vol. 58, No. 4, 2022, pp. 2660–2672. <https://doi.org/10.1109/TAES.2021.3135484>, URL <https://ieeexplore.ieee.org/document/9650527/>.
- [16] Song, Y., Wang, Y., Holloway, J., and Krstic, M., “Time-varying feedback for regulation of normal-form nonlinear systems in prescribed finite time,” *AUTOMATICA*, Vol. 83, 2017, pp. 243–251. <https://doi.org/10.1016/j.automatica.2017.06.008>, URL <https://linkinghub.elsevier.com/retrieve/pii/S000510981730290X>, num Pages: 9 Place: Oxford Publisher: Pergamon-Elsevier Science Ltd Web of Science ID: WOS:000408288800028.
- [17] Wang, Y., Song, Y., Hill, D. J., and Krstic, M., “Prescribed-Time Consensus and Containment Control of Networked Multiagent Systems,” *IEEE Transactions on Cybernetics*, Vol. 49, No. 4, 2019, pp. 1138–1147. <https://doi.org/10.1109/TCYB.2017.2788874>, URL <https://ieeexplore.ieee.org/document/8272410>.
- [18] Cao, Y., Cao, J., and Song, Y., “Practical prescribed time tracking control over infinite time interval involving mismatched uncertainties and non-vanishing disturbances,” *Automatica*, Vol. 136, 2022, p. 110050. <https://doi.org/10.1016/j.automatica.2021.110050>, URL <https://www.sciencedirect.com/science/article/pii/S0005109821005781>.
- [19] Zhang, K.-K., Zhou, B., and Duan, G.-R., “Global prescribed-time output feedback control of a class of uncertain nonlinear systems by linear time-varying feedback,” *Automatica*, Vol. 165, 2024, p. 111680. <https://doi.org/10.1016/j.automatica.2024.111680>, URL <https://www.sciencedirect.com/science/article/pii/S0005109824001742>.
- [20] Zhao, S., Zheng, J., Yi, F., Wang, X., and Zuo, Z., “Exponential Predefined Time Trajectory Tracking Control for Fixed-Wing UAV With Input Saturation,” *IEEE Transactions on Aerospace and Electronic Systems*, Vol. 60, No. 5, 2024, pp. 6406–6419. <https://doi.org/10.1109/TAES.2024.3402656>, URL <https://ieeexplore.ieee.org/document/10534850/>.

- [21] Xiao, Y., Yang, Y., Ye, D., and Zhao, Y., “Scaling-Transformation-Based Attitude Tracking Control for Rigid Spacecraft With Prescribed Time and Prescribed Bound,” *IEEE Transactions on Aerospace and Electronic Systems*, Vol. 61, No. 1, 2025, pp. 433–442. <https://doi.org/10.1109/TAES.2024.3451454>, URL <https://ieeexplore.ieee.org/document/10659135>.
- [22] Zhou, B., Michiels, W., and Chen, J., “Fixed-Time Stabilization of Linear Delay Systems by Smooth Periodic Delayed Feedback,” *IEEE Transactions on Automatic Control*, Vol. 67, No. 2, 2022, pp. 557–573. <https://doi.org/10.1109/TAC.2021.3051262>, URL <https://ieeexplore.ieee.org/document/9321518>.
- [23] Ding, Y., Zhou, B., Zhang, K.-K., and Michiels, W., “Strong Prescribed-Time Stabilization of Uncertain Nonlinear Systems by Periodic Delayed Feedback,” *IEEE Transactions on Automatic Control*, Vol. 69, No. 6, 2024, pp. 4072–4079. <https://doi.org/10.1109/TAC.2023.3347703>, URL <https://ieeexplore.ieee.org/document/10375772>.
- [24] Zhou, B., Ding, Y., Zhang, K.-K., and Duan, G.-R., “Prescribed time control based on the periodic delayed sliding modesurface without singularities,” *SCIENCE CHINA Information Sciences*, Vol. 67, No. 7, 2024. <https://doi.org/10.1007/s11432-023-4052-4>, URL <https://www.scienceengine.com/10.1007/s11432-023-4052-4>, publisher: Science China Press.
- [25] Kobayashi, H., Shoji, Y., and Yamada, K., “Optimal Attitude Trajectory of Spacecraft with Pyramid-Type CMGs Using a Pseudo-Spectral Method,” *AEROSPACE TECHNOLOGY JAPAN, THE JAPAN SOCIETY FOR AERONAUTICAL AND SPACE SCIENCES*, Vol. 16, No. 0, 2017, pp. 55–63. <https://doi.org/10.2322/astj.16.55>, URL https://www.jstage.jst.go.jp/article/astj/16/0/16_JSASS-D-16-00034/_article/-char/ja/.
- [26] Spiller, D., Melton, R. G., and Curti, F., “Inverse dynamics particle swarm optimization applied to constrained minimum-time maneuvers using reaction wheels,” *Aerospace Science and Technology*, Vol. 75, 2018, pp. 1–12. <https://doi.org/10.1016/j.ast.2017.12.038>, URL <https://www.sciencedirect.com/science/article/pii/S1270963817308684>.
- [27] Celani, F., and Lucarelli, D., “Spacecraft Attitude Motion Planning Using Gradient-Based Optimization,” *Journal of Guidance, Control, and Dynamics*, Vol. 43, No. 1, 2020, pp. 140–145. <https://doi.org/10.2514/1.G004531>, URL <https://arc.aiaa.org/doi/10.2514/1.G004531>, publisher: American Institute of Aeronautics and Astronautics.
- [28] Tao, H. U. O., Jin, Y., Chengfei, Y. U. E., Xueqin, C., and Xibin, C. a. O., “Gradient-based attitude planning for rigid spacecraft on $SO(3)$,” *SCIENCE CHINA Technological Sciences*, Vol. 68, No. 5, 2025. <https://doi.org/10.1007/s11431-024-2883-1>, URL <https://www.scienceengine.com/10.1007/s11431-024-2883-1>, publisher: Science China Press.
- [29] Chai, R., Tsourdos, A., Savvaris, A., Chai, S., Xia, Y., and Chen, C. L. P., “Six-DOF Spacecraft Optimal Trajectory Planning and Real-Time Attitude Control: A Deep Neural Network-Based Approach,” *IEEE Transactions on Neural Networks and Learning Systems*, Vol. 31, No. 11, 2020, pp. 5005–5013. <https://doi.org/10.1109/TNNLS.2019.2955400>, URL <https://ieeexplore.ieee.org/document/8939337>.
- [30] Gong, P., Yan, Z., Zhang, W., and Tang, J., “Lyapunov-based model predictive control trajectory tracking for an autonomous underwater vehicle with external disturbances,” *Ocean Engineering*, Vol. 232, 2021, p. 109010. <https://doi.org/10.1016/j.oceaneng.2021.109010>, URL <https://www.sciencedirect.com/science/article/pii/S0029801821004455>.

- [31] Patterson, M. A., and Rao, A. V., “GPOPS-II: A MATLAB Software for Solving Multiple-Phase Optimal Control Problems Using hp-Adaptive Gaussian Quadrature Collocation Methods and Sparse Nonlinear Programming,” *ACM Trans. Math. Softw.*, Vol. 41, No. 1, 2014, pp. 1:1–1:37. <https://doi.org/10.1145/2558904>, URL <https://dl.acm.org/doi/10.1145/2558904>.